

Chapter 2

Identifying pathway regulators and constructing RNA-based regulatory systems to control decision-making in the yeast mating pathway

Abstract

Synthetic biology is advancing capabilities in constructing genetic circuits that can program biological functions. However, the application of these circuits to the regulation of cell fate has been limited by the means to connect synthetic circuitry to the pathways that govern cellular decision-making. Identifying and controlling the expression of key pathway regulators represents one possibility for connecting synthetic circuits to the processes that govern cell fate. Here, we show that in a model MAPK pathway, the *Saccharomyces cerevisiae* mating pathway, there exist titratable positive and negative regulators of pathway activity and a narrow range of expression of these regulators over which cellular fate diverges. Synthetic circuits designed to control the levels of these regulators were able to divert cells to alternative fates even in the face of antagonistic external signals. By layering these circuits with small-molecule-responsive, RNA-based controllers, we constructed molecular network diverters that specify alternative cell fate decisions in response to exogenous environmental signals. The diverters are designed to remain quiescent in the absence of the environmental input, but activate in the presence of the input signal to route cells to one of two alternative mating fates: “chaste” or “promiscuous”. In wild type cells, pheromone stimulates the mating pathway, inducing cell cycle arrest. Cells exhibiting the chaste phenotype are insensitive to mating cues and do not arrest, whereas promiscuous cells exhibit upregulated signaling through the mating pathway and arrest in the absence of the canonical mating stimulus. Diverters that incorporate a positive feedback architecture enhanced switching to the promiscuous fate, whereas diverters incorporating negative feedback exhibited reduced population heterogeneity. The molecular network diverters control fate decisions without modifying

the host's native genetic material, obviating the need for laborious and potentially infeasible genetic manipulation. The modularity of this control scheme makes this technique broadly applicable to an extensive range of native networks such as those that govern stem cell fate and the establishment and proliferation of cancer.

Introduction

To orchestrate complex, coordinated, multicellular tasks, organisms dynamically program their extracellular space with distributed molecular signals that are processed by individual cells into concerted responses. These extracellular signals activate signaling cascades that induce specific network topologies, leading cells to divergent cellular fates. MAPK cascades are a class of highly conserved signaling pathways that control such key cellular processes as differentiation, mitosis, and apoptosis [1]. Many diseases, including one third of human cancers, result from aberrant signaling through MAPK pathways [2, 3]. In the model eukaryotic organism *Saccharomyces cerevisiae*, multiple MAPK cascades direct cellular fate via divergent regulatory programs. Decisions to upregulate gene expression, halt cell cycle, and change cell morphology are programmed through these pathways as the rational response to changing environmental signals.

The ability to dynamically modulate signaling through MAPK pathways in the face of antagonistic environmental stimuli represents an enormous hurdle in the reprogramming of cell fate decisions. Many of the current strategies for programming cell fate are based on strict control over the extracellular environment [4, 5], presenting limitations in clinical settings and necessitating the development of strategies that are more amenable to therapeutic contexts. Several modeling efforts have posited that levels of signaling molecules are responsible for divergent cell fates [6-8]. Further, experimental studies comparing wild-type response to overexpression and knockouts of signaling pathway components demonstrate that differential pathway activity and cell fate can be achieved via altering the expression levels of particular proteins [9-11]. However, these examples represent extreme perturbations to pathway response. We postulate that

within the continuum of regulator expression levels between wild type and high levels of ectopic overexpression there exists a transitory region over which cell fate diverges (Figure 2.1). In such a model, at subtransition levels of regulator expression, cells mirror the wild-type response. At expression levels above the requisite transitory range, cells adopt an alternative cell fate. By constructing synthetic circuits that can toggle between subtransition and supertransition levels of regulator expression, cellular behavior can be synthetically switched from wild type to programmed alternative fates.

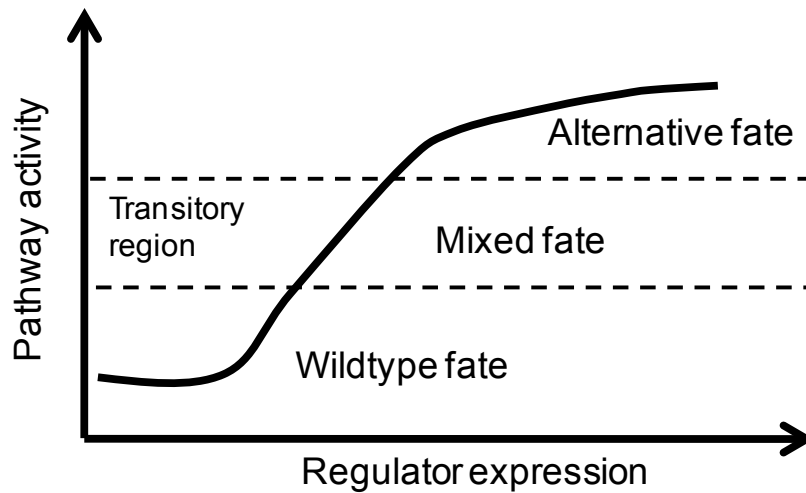


Figure 2.1. Regulator expression modulates pathway activity and over a narrow range of expression transitions to an alternative fate

We present a method for identifying and interfacing with control points in the *S. cerevisiae* mating and osmolarity response pathways. Using a galactose-responsive titration system, we successfully identified both a positive and a negative regulator in the mating pathway and two coexpressed positive regulators in the osmolarity pathway. The regulators of the mating pathway were shown to route cells to alternative fates above a particular threshold of expression. By incorporating these regulators into various network architectures with RNA-based controllers [12], we successfully constructed several types

of molecular network diverters in the mating pathway which conditionally route cells to one of two alternative cell fates based on the presence of distinct environmental signals. Our results demonstrate the utility of conditionally activated control systems for applications modulating cell growth and/or viability as well as the rational tuning of these synthetic circuits via the exchange of well-characterized parts. Further, we show that positive feedback reshapes the pathway activity response curve, shifting the threshold at which cell fate diverges to lower levels of the positive regulator. Finally, we have elucidated design principles and methodology for constructing molecular network diverters that can be readily extended to new pathways and applications.

Results

Identifying key pathway regulators that allow routing of cell fate decisions to alternative phenotypes in the mating pathway

S. cerevisiae activates a three-tiered MAPK cascade upon stimulation with pheromone that upregulates transcription of mating genes, induces cell cycle arrest, and initiates polarized cell growth characteristic of the mating response [8-9] (Figure 2.2). To identify regulators of pathway activity, we individually titrated the levels of signaling proteins in the pathway via an engineered galactose-inducible promoter system (*pGALI*), which allows for linear, homogeneous regulation of a target gene [13] (Supplementary Figure 2.1). The engineered strain allowed us to identify key pathway regulators by interrogating the effect of titrating mean protein expression levels on pathway activity. We used these strains to determine if overexpression of the regulators was sufficient to cross the transitory range to mediate routing to an alternative fate. Pathway activity was

measured by monitoring expression from a transcriptional fusion construct (*pFUS1*-GFP, GFP fused to a mating responsive promoter), where GFP levels represent a measure of pathway activation, and by observing mating-associated cell cycle arrest via halo assays (see Materials and methods).

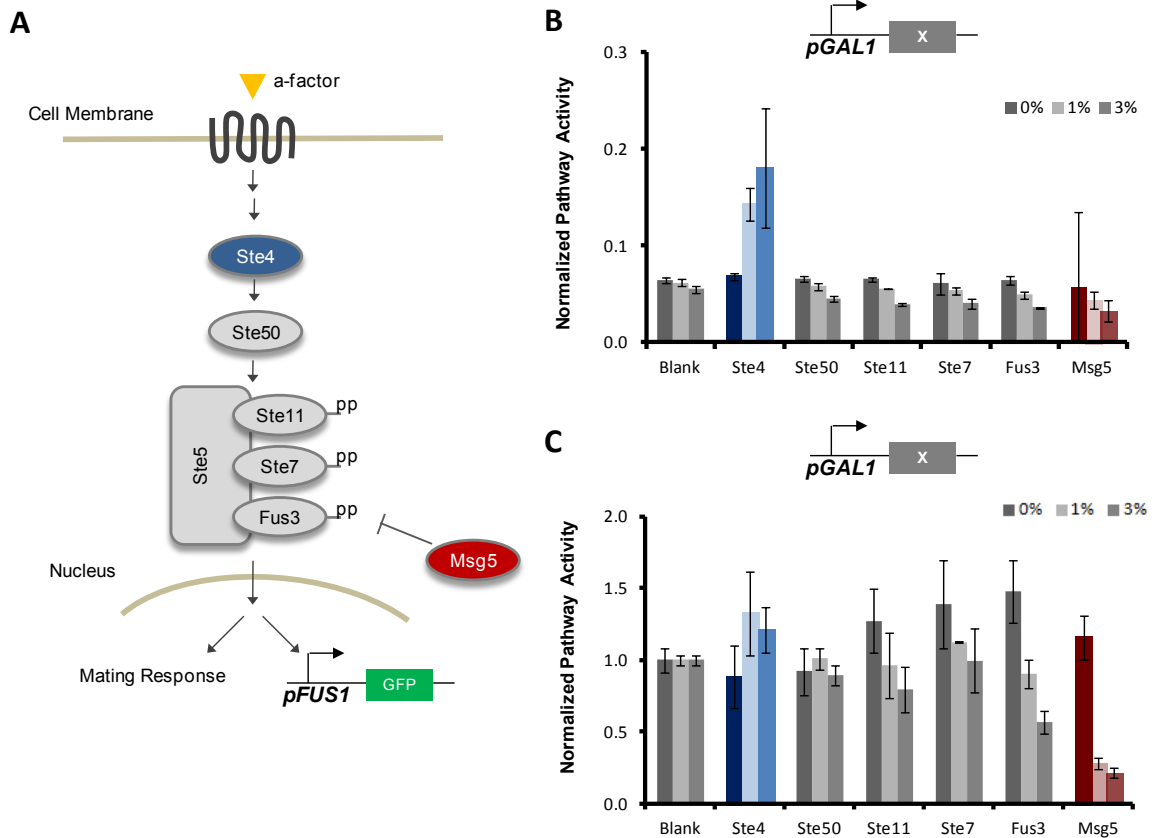


Figure 2.2. Identifying titratable regulators of pathway activity in the yeast mating pathway. **A.** A molecular view of signaling in the yeast mating pathway. Pheromone (α -factor) binds to a transmembrane receptor to initiate signaling. That binding event is transduced across the cell membrane and relayed down to the G-proteins including, Ste4 and Ste50, an adaptor protein, that in turn relay signaling to the Ste5 scaffold-bound three-tiered MAPK cascade. Phosphorylation of the MAPK Fus3 results in its translocation to the nucleus and is antagonized by the phosphatase Msg5. Fus3 translocation activates a host of transcription factors which ultimately upregulate expression at various mating gene including FUS1. Pathway activity can be monitored via an integrated *pFUS1*-GFP promoter fusion. Additionally, the mating response is characterized by pheromone-induced cell cycle arrest and polarized cell growth called shmoo formation. **B.** To find pathway activators, cells were monitored in the absence of stimulating pheromone. Ste4 increased pathway activity in a galactose-dependent manner indicating it is a titratable regulator. **C.** To find pathway inhibitors, the pathway was stimulated with pheromone. Msg5 overexpression reduced stimulated pathway activity. Cells were cultured in 0, 0.25 and 1% galactose for 6 hours. Pheromone was added 3 hours post-dilution to stimulate the pathway. Pathway activity was monitored via flow cytometry measurement of cellular fluorescence of GFP from the promoter fusion *pFUS1*-GFP.

Only two of the six pathway proteins examined in this system exhibit significant effects as positive or negative regulators (Figure 2.2B, C). Overexpression of *Msg5* from the engineered galactose-titratable promoter system results in a decrease in pathway activation, as measured from the *pFUS1*-GFP reporter construct, and over a threshold level *Msg5* eliminates pheromone-induced cell cycle arrest, as demonstrated by halo assays (Figure 2.3A, B). Conversely, *Ste4* overexpression increases pathway activation and reduces cell growth (Figure 2.3D, E). For both regulators, phosphorylated levels of the MAPK *Fus3* correlated with GFP levels and cell fate, indicating that the synthetic circuits act through the canonical signaling pathway (Figure 2.3C, F). While previous work supports the role of *Msg5* and *Ste4* as negative and positive regulators of pathway activity [10, 14], respectively, we have demonstrated that these regulators modulate pathway activity in a dose-dependent manner and above a particular threshold of expression each regulator directs cell fate away from the wild-type response to an alternative phenotype. High levels of *Msg5* inhibit pathway activation in the presence of pheromone, routing cells to a “chaste” fate. Above a threshold level of *Ste4*, cells constitutively activate the pathway in the absence pheromone to adopt a “promiscuous” fate. Our identification of only two pathway regulators from this screen supports the hypothesis that within many signaling pathways regulatory architectures filter out perturbations in the expression of signaling components [15, 16]. However, despite the native control schemes, we identified two control points where overexpression of the regulatory proteins dictates the level of pathway activity.

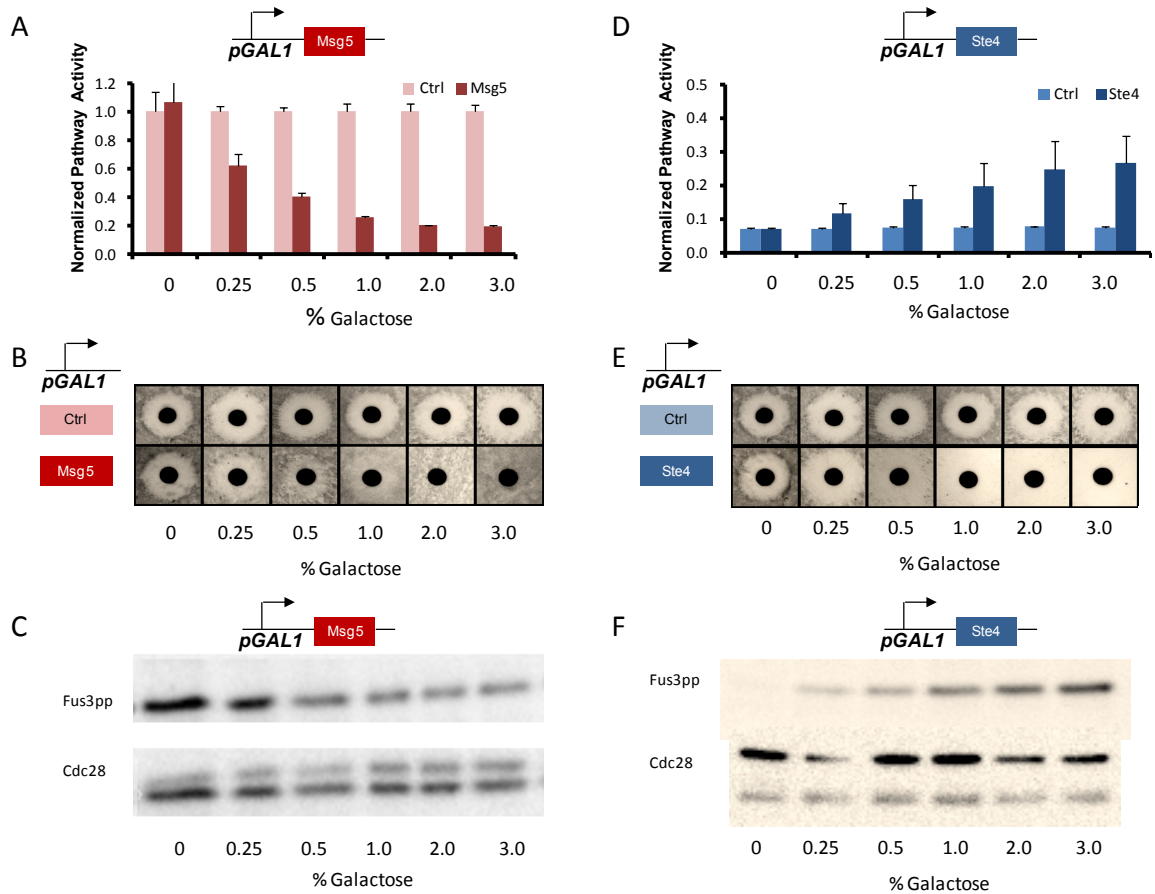


Figure 2.3. Overexpression of Msg5 and Ste4 modulates pathway activity and routes cells to an alternative fate. **A.** Increasing Msg5 overexpression results in reduced pathway activity over the galactose range as measure by pFUS1-GFP levels **B.** Halo assays at various concentrations of galactose indicate that as galactose concentration increases Msg5 overexpression inhibits pheromone-induced cell cycle arrest leading to a “chaste” phenotype. **C.** Phosphorylated levels of Fus3 correspondingly drop across the galactose range while the Cdc28 control levels remain constant. **D.** For Ste4 overexpression, pathway activity increases as galactose levels increase. **E.** Halo assays at various concentrations of galactose indicate that as galactose concentration increases Ste4 overexpression generates pheromone-independent cell cycle arrest or “promiscuous” fate. **F.** Phosphorylated levels of Fus3 correspondingly drop across the galactose range while the Cdc28 control levels remain constant.

Identifying pathway regulators in the osmolarity pathway

To examine the flexibility of the synthetic titration system for identifying pathway regulators, we applied it to a second yeast MAPK pathway, the osmolarity response pathway. The osmolarity response is triggered by high osmotic pressure that initiates signaling at two different receptors Sho1 and Sln1, which converge on a three-tiered

MAPK cascade (Figure 2.4A). Signaling results in phosphorylation and translocation of the dedicated osmo-MAPK Hog1 to the nucleus, and ultimately upregulation of osmo-genes and production of glycerol. Activation of the osmolarity response is also known to repress the mating pathway. We used the engineered galactose-inducible strain to evaluate the potential of several signaling proteins as titratable positive pathway regulators. Negative regulators were not explored with this method as inhibiting the osmolarity pathway in yeast challenged with high osmotic pressure results in cell death [17].

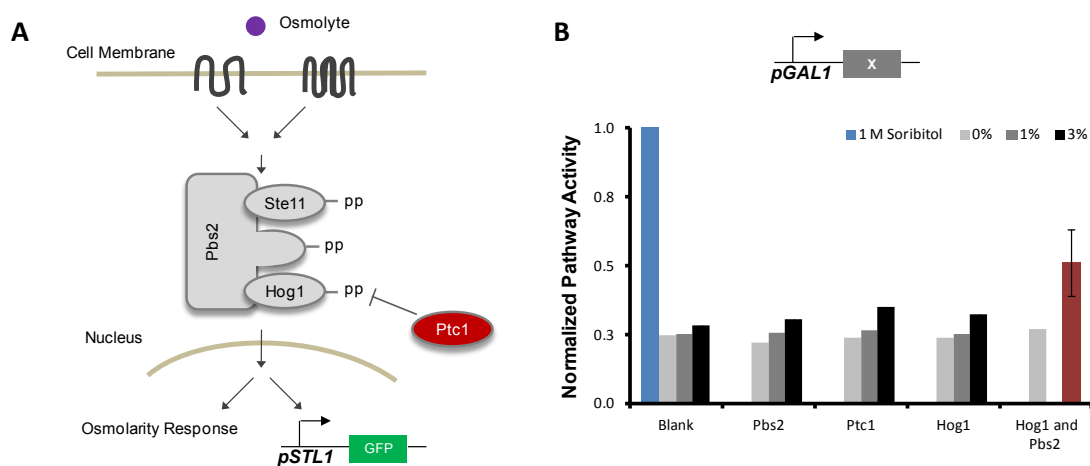


Figure 2.4. Identifying titratable regulators in the yeast osmolarity pathway. **A.** A molecular view of signaling in the yeast osmolarity pathway. High osmotic pressure initiates signaling via two transmembrane sensor proteins. Signaling is relayed to the Pbs2 scaffold-bound three-tiered MAPK cascade. Phosphorylation of the MAPK Hog1 results in its translocation to the nucleus and is antagonized by the phosphatase Ptc1. Hog1 translocation activates a host of transcription factors which ultimately upregulate expression at various osmo genes including STL1. Pathway activity can be monitored via an integrated pSTL1-GFP promoter fusion. Additionally, the osmolarity response is characterized by glycerol production. **B.** Increasing pathway activity in the osmolarity pathway requires overexpression of both Hog1 and Pbs2. To find pathway activators, cells were monitored in the absence of sorbitol. Cells were cultured in 0, 1, and 3% galactose for 6 hours. Pathway activity was monitored via flow cytometry measurement of cellular fluorescence of GFP from the promoter fusion pSTL1-GFP.

The impact of overexpression of three pathway proteins on osmolarity pathway activation was examined using the galactose-titratable expression system. Pathway activation was measured via a transcriptional fusion between a promoter that is activated through osmolarity pathway stimulation and GFP (*pSTL1*-GFP). Even at high induction

levels, the overexpression of single pathway proteins resulted in very small increases in pathway activation (Figure 2.4B). We hypothesized that co-overexpressing both the scaffold-kinase, Pbs2, and the MAPK Hog1 would lead to more substantial increases in pathway activity. We observed that co-overexpression of Pbs2 and Hog1 significantly increased pathway activation over single component expression.

Evaluating whether an alternative phenotypic fate can be achieved by controlling activation of the osmolarity pathway via regulator overexpression encountered several challenges. First, unlike the mating pathway (e.g., cell cycle arrest) the osmolarity pathway does not have a well-defined phenotypic readout. As a proxy, Hog1 translocation to the nucleus has been used as a measure of pathway activation using a strain composed of a fluorescently labeled Hog1 and nuclear protein marker [18]. In the native pathway, Hog1 translocation occurs rapidly following hyperosmotic shock and pathway activity attenuates within minutes, returning nuclear Hog1 levels to pre-stimulated levels. This timing dependence poses an issue in determining when to assay Hog1 translocation for our system in which the pathway is not stimulated by osmotic shock but instead by overexpression of protein components established over the course of the 6 hour assay. Similar issues are associated with evaluating phosphorylated Hog1 as a measure of pathway activity since the phosphorylation time scale mirrors that of translocation. Due to the challenges associated with determining fate from pathway activation, we did not perform this evaluation for the engineered systems. With significant method development it may be possible to evaluate fate routing in the osmolarity pathway. However, in light of the time scale of action for the osmolarity response, transcriptional feedback control may not be aptly suited to controlling the

osmolarity pathway. Under such time scale constraints, transcriptional control systems may modulate the initial conditions that guide the response, but dynamic modulation of signaling via feedback would be necessarily precluded.

Building molecular network diverters for programming cell fate decisions

A molecular network has a particular topology which shapes the flow of signal in the pathway. Reshaping the network in decision-making pathways, such as MAPK pathways, offers the potential to divert the endogenous response to an alternative fate. Network reshaping requires identifying and plugging into a network regulatory node, a sensitive control point in the pathway for directing pathway activity and fate. Pathway regulators govern the function of their cognate regulatory nodes. Changes in the native network shape can be induced by raising the profile of a pathway regulator. A molecular network diverter conditionally routes cells to an alternative fate by transducing signals in the environment into changes in network shape via the modulation of the pathway regulator profile (Figure 2.5). A molecular network is composed of a switch which encodes a sensing function that recognizes the environmental signal. Increasing the input concentration increases the signal transduced to the actuator element within the switch (Figure 2.5A). The activity of the actuator combined with the strength of the modulator dictates the profile of the pathway regulator. As the concentration of the environmental input increases, the profile of the imbedded pathway regulator rises. Once the profile exceeds a particular threshold, the regulator docks to the network regulatory node and induces changes in the native molecular network, diverting the pathway response (Figure 2.5B).

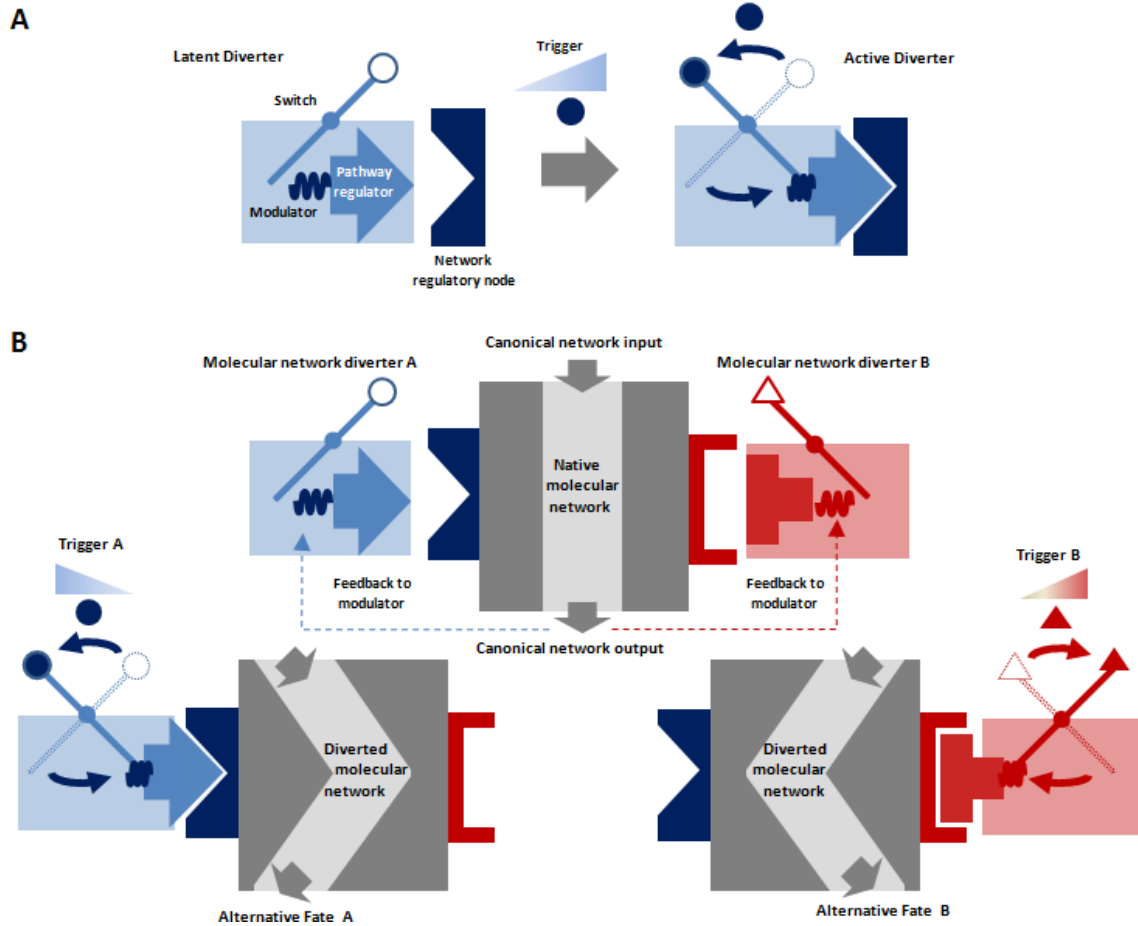


Figure 2.5. Reshaping the native molecular network with molecular network diverters. **A.** The latent diverter is activated by increasing trigger concentrations with flip the switch which raises the profile of the pathway regulator via the modulator. Above a certain threshold, the pathway regulator docks to the regulatory node to reshape the native network. **B.** Trigger binding to its cognate sensor flips the switch. Binding is transduced via the switch actuator to the modulator and finally to the imbedded pathway regulator, raising the profile of the regulator which plugs into its cognate regulatory node, reshaping the molecular network and diverting fate. The diverter function can be tuned by the properties of the switch, the modulator, and addition of feedback to the modulator.

The properties of the molecular network diverter can be tuned via the genetic parts selected to compose the diverter. The diverter's component functions can be mapped to particular genetic parts (Figure 2.6). The modulator maps to a promoter, where the promoter strength determines how strongly changes in the activity of the switch actuator are translated into changes in the profile of the pathway regulator. For the mating pathway, the pathway regulator is a gene cassette encoding either Ste4 or Msg5. The switch maps to RNA-based controllers.

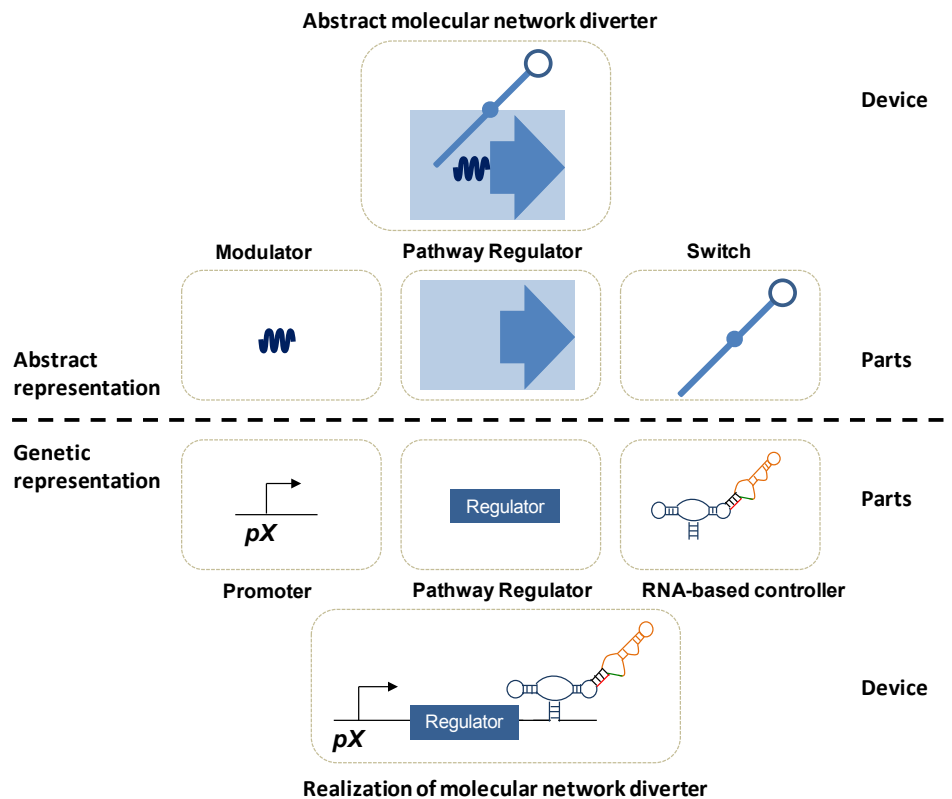


Figure 2.6. Implementation of a molecular network diverter from various genetic parts. The molecular network diverter is composed with a modulator, pathway regulator, and a switch into the larger device. Mapping these parts to their genetic representation, the modulator is a promoter, the pathway regulator is a gene that regulates pathway activity, and the switch is an RNA-based controller. Assembling the genetic parts in the proper configuration allows the realized molecular network diverter to conditionally regulate pathway activity and divert cell fate.

Construction of a molecular network diverter requires the selection of regulatory elements with the appropriate strength and range for modulating the pathway regulator levels to conditionally route cellular fate. The selection of the promoter driving the expression of the regulator is a key component in setting the activity of the molecular network diverter. Constitutive promoters of varying strength achieve different levels of regulator expression (Figure 2.7). The pathway activity response curve indicates where a promoter-regulator pair falls on this curve, which dictates whether cells route to the wild-type or alternative fate. Using a promoter responsive to pathway activation results in the construction of a feedback molecular network diverter. Feedback in molecular networks

can be used to change the shape of the pathway activity response curve. Negative feedback has been shown to antagonize ultrasensitivity, converting sigmoidal responses to linear responses [19]. Positive feedback architectures can be used to establish ultrasensitivity, reducing the threshold of expression required to trigger switching to an alternative fate [20]. The strength of positive feedback represents a sensitive control point, which dictates whether cells adopt the wild-type or alternative fate. We used four constitutive promoters of varying strength and a feedback promoter to construct and evaluate molecular network diverters (Supplementary Figure 2.2).

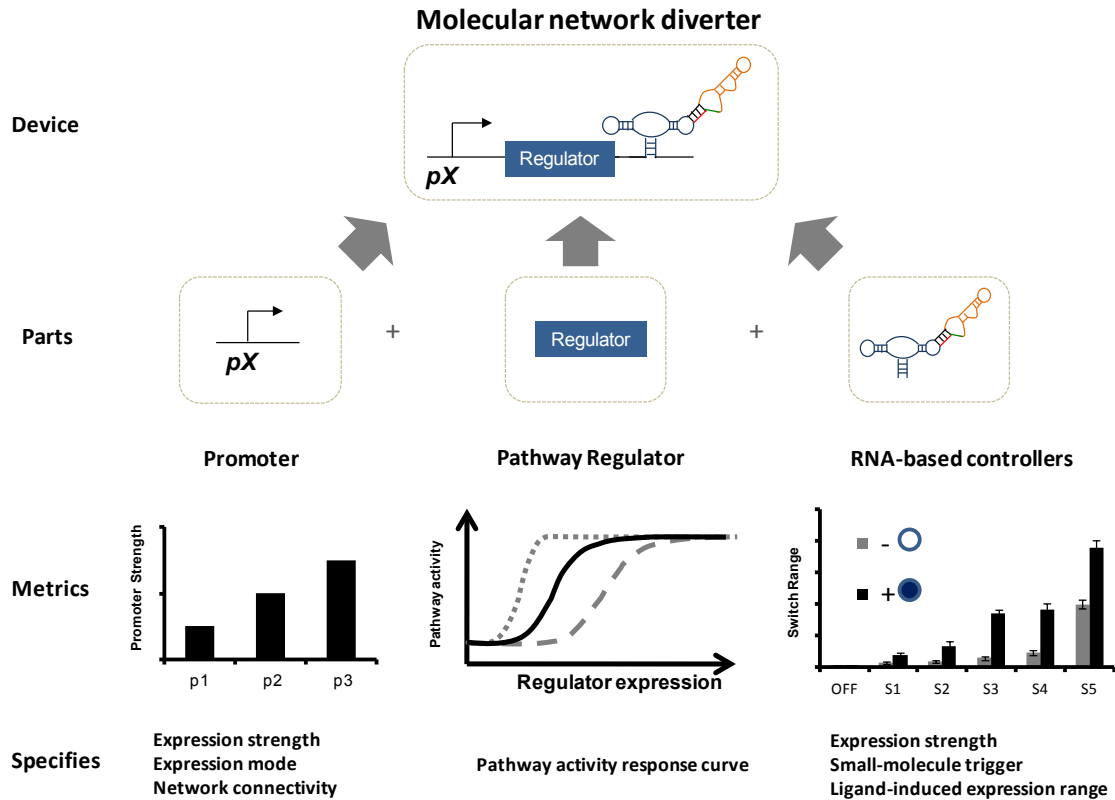


Figure 2.7. Composition of a molecular network diverter from well-defined parts. The molecular diverter is composed of a promoter, a pathway regulator, and a RNA-based controller, also called a switch. The promoter specifies the expression mode (e.g., constitutive or feedback) which determines the network connectivity. The promoter and switches combine to determine the expression strength and thus the activity of the diverter. The pathway regulator's interaction with the native molecular network determines the pathway response curve. The pathway response curve can be altered by changes in network connectivity due to feedback expression of regulators. Switches specify which small-molecule input regulates expression and the range of expression across ligand concentrations.

RNA controllers provide a second layer of control by which to tune pathway regulator levels and allow the molecular network diverter to respond to environmental signals. Small-molecule-responsive RNA-based controllers, also called RNA switches, are an engineered class of noncoding RNA that allows for conditional control from any promoter-gene pair via a chemical trigger [12]. The RNA switches act post-transcriptionally to destabilize transcripts in an input-dependent manner, thereby upregulating or downregulating target protein levels in response to increasing concentrations of environmental triggers. The regulated output achieved by these programmable RNA controllers spans a wide window of dynamic ranges and regulatory stringencies (Supplementary Figure 2.3). The switches used in this study respond to one of two chemical triggers, allowing for two independent channels through which to simultaneously regulate *Msg5* and *Ste4* expression. The relative switch regulatory activity is independent of other circuit components (e.g., gene, promoter) such that the activity relative to the ON state control (nonswitching) is expected to be consistent across different promoter-gene pairs, supporting rational programming of the molecular network diverter properties. The ON and OFF state controls (nonswitching) demark the highest and lowest potential expression levels, respectively, from a promoter-gene pair coupled to the RNA-based controllers. Since the ON and OFF state expression levels of the RNA switches fall within these extrema, differential fates from the controls must be observed in order to construct molecular network diverters that alter cell fate decisions (Figure 2.8).

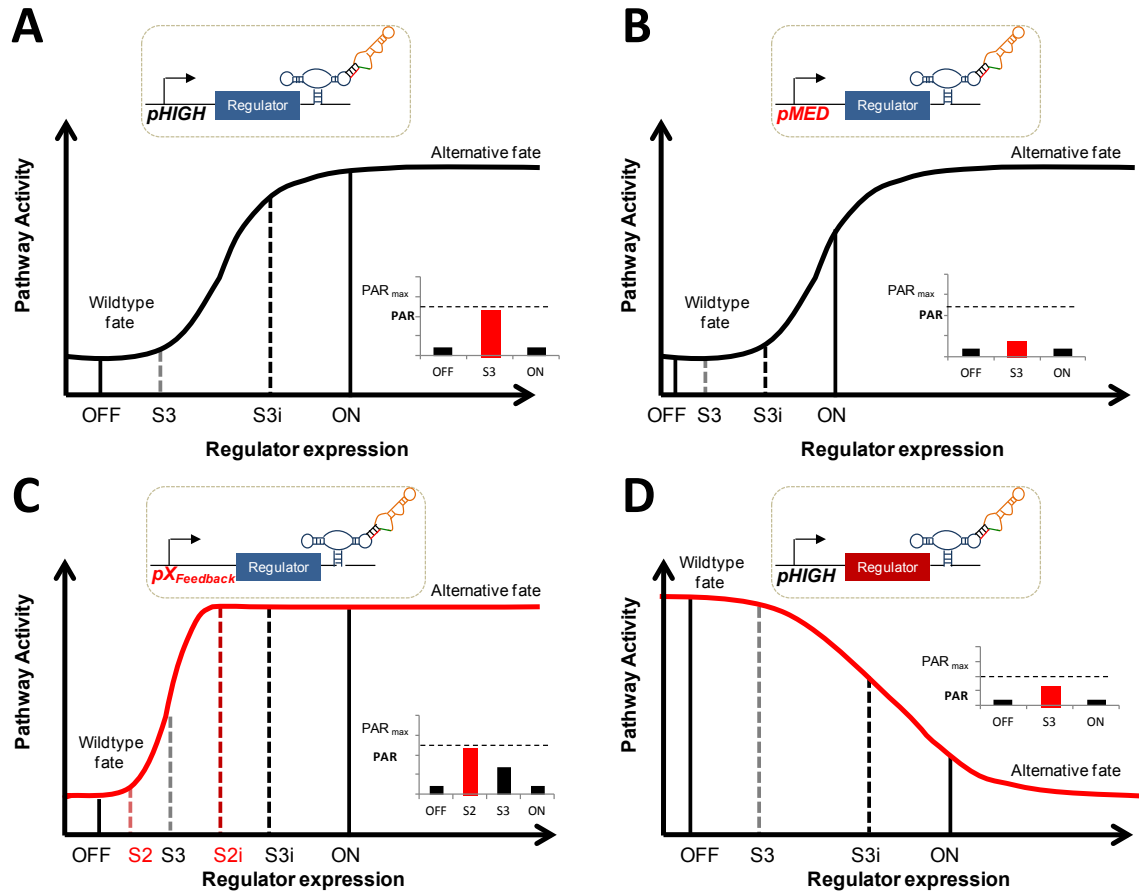


Figure 2.8. Optimal configuration of the molecular network diverter requires tuning via the selection of components with the requisite metrics. **A.** An optimally configured diverter spans the steep linear range of the pathway response curve to yield a PAR value approaching PAR_{max} . Switch S3 in the absence of input maintains the wild-type fate with low pathway activity (grey dashed line). With the addition of input (S3i), S3 switches to high pathway activity routing to the programmed alternative fate (black dashed line). **B.** Reducing the promoter strength results in a suboptimally configured diverter. **C.** Implementing feedback expression of a positive regulator introduces ultrasensitivity. As a result, a more stringent switch (with lower basal levels) is required to achieve optimal diverter performance. **D.** Substituting a negative regulator for a positive regulator enables construction of a negative diverter. The negative diverter attenuates activity in the stimulated pathway. PAR (pathway activation ratio) is the ratio of the pathway activity in the presence and absence of the input for positive diverters. For negative diverters, PAR is the inverse of this ratio.

A molecular network diverter requires that regulator expression spans the transitory range such that expression is above the requisite threshold in the presence of the input signal, while sub-transition levels are maintained in the absence of the signal. Optimal performance of the molecular network diverter requires tuning via the selection of components with the requisite metrics (Figure 2.8). In an optimally configured

diverter, the switch maintains wild-type behavior in the absence of environmental input and routes to the alternative fate in the presence of the input (Figure 2.8A). The efficiency of the molecular network diverter's response to the input signal is measured by the pathway activation ratio (PAR), the ratio of the pathway activity in the presence and absence of the input for positive diverters. For negative diverters, PAR is the inverse of this ratio. An optimally configured diverter spans the steep linear region of the pathway response curve, resulting in a PAR value approaching PAR_{max} . For positive diverters, PAR_{max} is the ratio of the maximum to minima of the response curve as shown for S3 (Figure 2.8A, inset); for negative diverters, PAR_{max} is the inverse ratio.

The modular components within the molecular network diverter architecture provide an array of tools for tuning the activities of these controllers to best interface with endogenous cellular networks. For example, changing the promoter in the regulator-switch pair can significantly alter the diverter's PAR value (Figure 2.8A, B). Additionally, the introduction of positive feedback into the network diverter architecture can result in shifts to the response curve that introduce ultrasensitivity and ultimately require more stringent RNA controllers to achieve optimal PAR values (Figure 2.8C). As another example, exchanging a positive pathway regulator in a positive network diverter for a negative regulator enables the construction of a negative network diverter in which activity is attenuated (Figure 2.8D).

Engineering a positive molecular network diverter that conditionally routes cells to a “promiscuous” phenotype

To construct a positive molecular network diverter, we paired Ste4 with the four constitutive promoters of varying strength (Supplementary Figure 2.2) and the ON state control and evaluated the pathway response. For the three lower promoter strengths, cells weakly adopt a promiscuous fate characterized by diminished growth relative to cells harboring a control construct that lacked Ste4. Cells transformed with a construct harboring Ste4 under the control of the strongest promoter repeatedly failed to produce colonies. No phenotypic differences emerge across the range of the three lower promoter strengths examined (Supplementary Figure 2.4A). We paired pHIGH-Ste4 with tetracycline-responsive switches and nonswitch controls to determine the pathway response curve to regulator expression and the potential for phenotypic switching from this molecular network diverter architecture. Mild input-triggered phenotypic switching from wild-type to a promiscuous phenotype was observed from switch S4tc (Figure 2.9A). In contrast, no phenotypic switching was observed from any of the diverters in which the lower strength promoter, pLOW, was paired with Ste4 (Supplementary Figure 2.4B). We postulated that feedback expression of Ste4 might yield more robust phenotypic switching by introducing ultrasensitivity into the pathway response curve and by reinforcing pathway activation. The introduction of feedback expression of Ste4 into the network diverter architecture generated strong phenotypic switching from two tetracycline-responsive switches, S3tc and S4tc (Figure 2.9B).

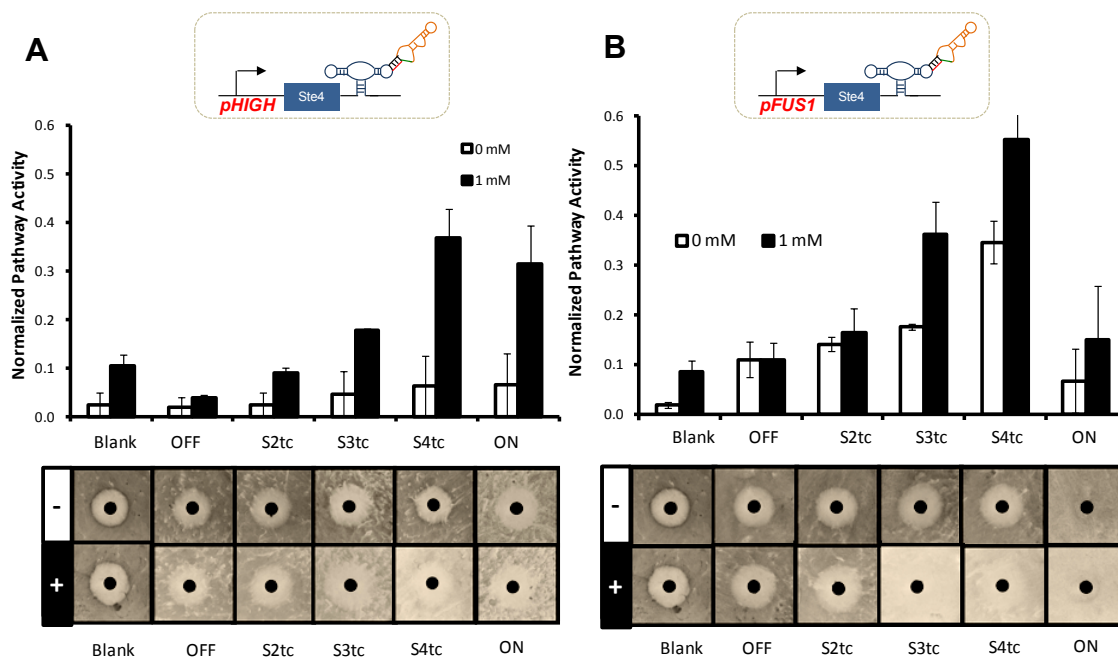


Figure 2.9. Tetracycline-inducible positive network diverters of different architectures conditionally route cells to the promiscuous phenotype. A. Pairing tetracycline-inducible switches of increasing strength with constitutive expression of Ste4 results in increasing levels of pathway activity. Addition of tetracycline increases pathway activity for each switch construct. For S4tc, plate assays in the absence of tetracycline show a wild-type halo, while at 1 mM tetracycline cells adopt the promiscuous phenotype. **B.** Constructing a positive feedback loop amplifies ligand-induced phenotype switching. S3tc and S4tc show wild-type halos in the absence of tetracycline and a strong promiscuous response to tetracycline with nearly undetectable levels of cellular growth.

A second set of diverters were composed from theophylline-responsive switches in both expression modes to demonstrate that routing via the molecular network diverters can be adapted to different target small-molecule inputs. Similar trends were observed between the tetracycline and theophylline-responsive switches. As expected, switches with similar basal levels and ranges achieve similar pathway activities and routing capabilities indicating the routing effect is independent of the specific identity of the input signal (Supplementary Figure 2.5). Further, the data support the ability to rationally tune molecular network diverters by the exchange of modular, well-defined parts.

The data also suggest important tradeoffs between activity and timing in constructing programs that modulate cellular growth. For example, the ON state control

for feedback expression of Ste4 exhibited significant growth despite being programmed for constitutive arrest. We postulated that strong Ste4 overexpression can place selective pressure against cells with highly active pathways, such that over time the population is dominated by cells resistant to pathway activation. Consequently, cells harboring these programs display a low pFUS1-GFP profile and exhibit growth within the expected halo region indicating resistance to pheromone-induced cell cycle arrest. At superthreshold feedback strengths, only cells resistant to activation of the mating program and/or the synthetic positive feedback loop are selected over time. To test this theory, we observed the behavior and GFP profile of cells harboring the feedback molecular network diverters in the presence and absence of the trigger molecule over time. The GFP profiles of cells harboring pFUS1-Ste4-S4tc dropped when grown in the presence of tetracycline for two days in contrast to cells grown in the absence of tetracycline (Supplementary Figure 2.6A). The plasmid marker levels measured via a constitutively expressed mCherry cassette showed normal variation across the samples. Thus, the mCherry levels did not show a correlation with pathway activity, indicating the plasmid is maintained at similar levels in cells grown in the absence or presence of tetracycline (Supplementary Figure 2.6B). Additionally, uniform growth across the plate in halo assays indicates that cells grown at superthreshold levels over an extended time are resistant to pheromone-induced cell cycle arrest (Supplementary Figure 2.6C). Above a threshold level of pFUS1-Ste4 expression only cells with minimal pathway activity escape persistent cell cycle arrest. These data suggest that the ultrasensitivity introduced by the positive feedback architecture lowers the threshold to activation, capturing nearly the entire population in the high activity region of the curve and broadly enforcing a strong selective pressure

against pathway activation. Ultrasensitivity is not introduced into cells programmed with constitutive expression of Ste4, potentially explaining why similarly strong resistance to mating is not observed in cells harboring network diverters encoding constitutive Ste4 expression. These results highlight the utility of programs that run quiescently until activated for applications in which the program necessarily modulates cellular processes such as growth rate and/or viability.

By compiling the pathway activity data for Ste4, we determined the pathway response curve to varying Ste4 levels, identified the transitory range across which cell fate diverges, and examined differences between constitutive and feedback expression of Ste4 observed in the traces of the pathway response curve. For constitutive expression of Ste4, we traced pathway activity as a function of the calculated Ste4 expression and identified the transitory range over which cell fate diverges. The data points show a steady increase in pathway activity with increasing Ste4 expression up to a threshold followed by a precipitous drop (Figure 2.10A). Only cells induced to super-threshold expression levels show high pathway activity as expected from results indicating that over time high Ste4 expression selects for mating resistant cells. The drop in pathway activity coincides with the divergence of fate observed in the halo assays (Figure 2.10B). For feedback expression, the transitory range resides at Ste4 expression levels that are almost four times lower than those for constitutive expression (Figure 2.10C, D). The results support our hypothesis that positive feedback introduces ultrasensitivity to the pathway response curve, shifting the threshold to lower Ste4 expression levels.

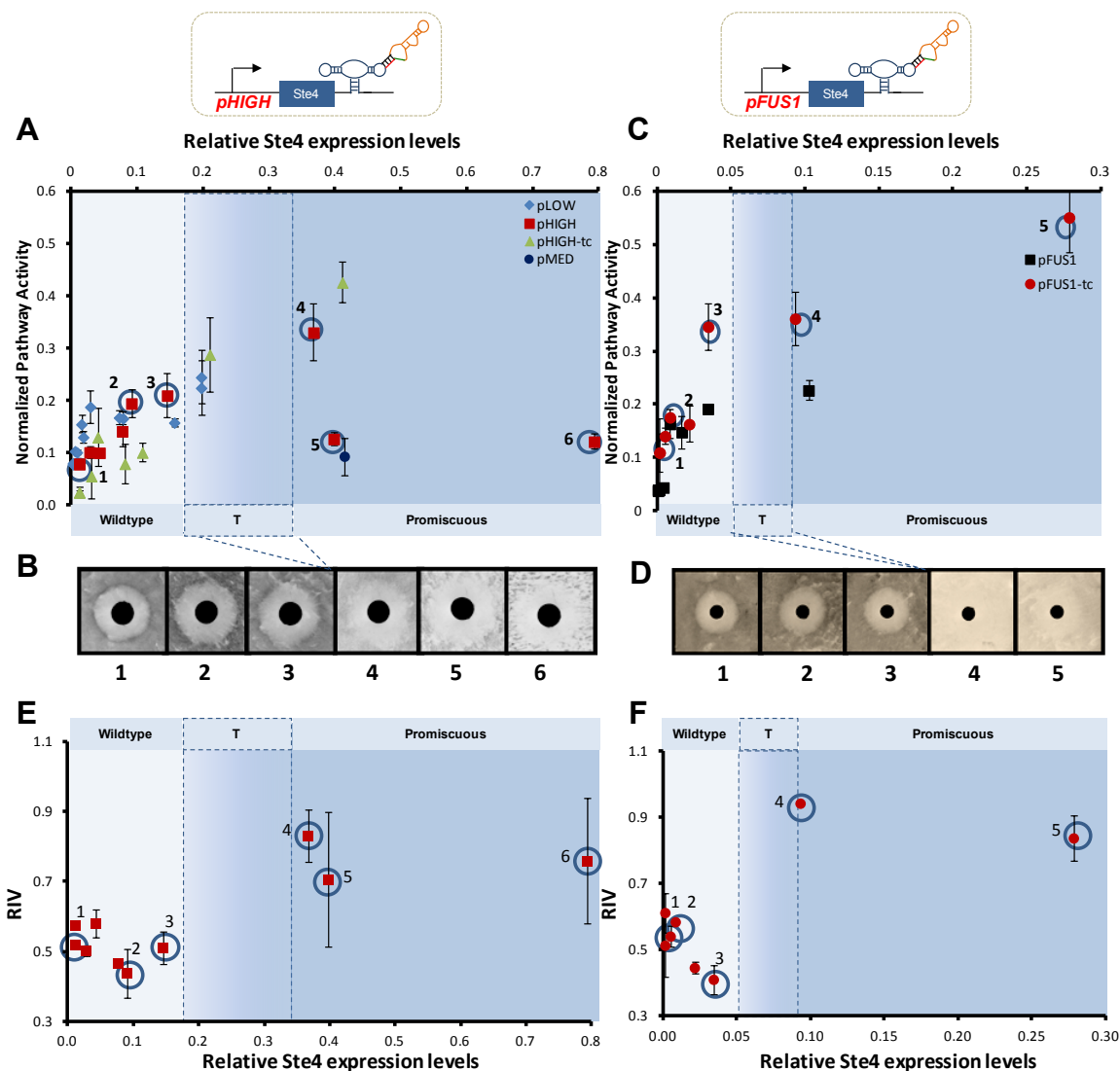


Figure 2.10. Tracing the pathway response curve of Ste4 expression to the promiscuous fate. **A.** Tracing the pathway response to constitutive Ste4 expression shows a steady increase in pathway activity with increasing relative Ste4 expression up to a threshold followed by a precipitous drop. Pathway activity increases from 2% to 35%. Above 40% expression, pathway activity drops (for calculated Ste4 expression levels see Materials and Methods). **B.** This drop coincides with the divergence of fate shown in the halo assays. Plate data correspond to points with numbered circles in A selected from the pHIGH-SX data set (Supplementary Figure 2.4). **C.** Tracing the pathway response with feedback Ste4 expression shows a narrower transitory range shifted to lower Ste4 expression levels. Pathway activity increases from 0% to 5%. Only samples induced with ligand show Ste4 levels above 10%. **D.** Above 10% Ste4 expression levels, plate assays show cells adopting the promiscuous fate. Plate data correspond to points with numbered circles in A selected from the pFUS1-SXtc data set (Supplementary Figure 2.9B). **E.** Relative intensity values (RIV) are low at low Ste4 expression levels and high at high Ste4 levels, indicating that the difference between inner and outer cell growth as measure by intensity is reduced above a particular level of Ste4 expression (see Methods for calculation of RIV). **F.** RIV values for feedback expression of Ste4 show two regimes of behavior. At low Ste4 expression, RIV values are low, but at high Ste4 expression cells transition to high RIV values indicating cells undergo pheromone-independent cell cycle arrest. “T” indicates transitory region.

We have demonstrated the construction of positive network diverters that route cells to the promiscuous fate. Additionally, we have shown that network diverters that incorporate a positive feedback architecture via a pathway responsive promoter exhibit enhanced fate switching compared to nonfeedback network diverter architectures controlling the same positive regulator, Ste4. Positive feedback loops are known to be important in developmental decision-making processes [21]. Thus, the described feedback molecular network diverters may provide insight into effective strategies for guiding the development of tissues from progenitor cells.

Building a negative molecular network diverter that conditionally routes cells to a “chaste” phenotype

A negative molecular network diverter was constructed by pairing *Msg5* with four promoters spanning a range of expression levels. We examined pathway activation in cells harboring these constructs under saturating pheromone conditions. Each construct exhibited routing to the chaste fate (Supplementary Figure 2.7). A set of negative network diverters of varying strength and range that are orthogonal to the positive diverters were constructed by pairing the strong promoter (*pHIGH*) and the theophylline-responsive switches (Figure 2.11A). Having constructed both tetracycline- and theophylline-responsive positive diverters, negative diverters responsive either small-molecule would provide for an orthogonal pair of diverters each responsive to its particular input signal. While we anticipate that tetracycline-responsive switches would mirror the phenotypic results observed with theophylline, we chose theophylline to regulate the negative diverter to mitigate any potentially confounding issues with *pFUS1*-

GFP analysis associated with tetracycline autofluorescence. The low expression level of *Msg5* associated with the OFF state control allowed pathway activation in the presence of pheromone, leading to high GFP levels, a low PAR value, and wild-type halo formation (Figure 2.11B, C, D). In contrast, the high expression level of *Msg5* associated with the ON state control inhibited pheromone-induced pathway activation, thereby eliminating cell cycle arrest and resulting in low GFP levels. Between S2 and S4 cell fate diverges from the wild-type to chaste phenotype. The basal expression levels of *Msg5* associated with S1 and S2 in the absence of theophylline are sufficiently low to permit elevated pathway activity in response to pheromone and the characteristic halo formation as is observed for the OFF state control. Both S1 and S2 attenuated pathway activity in the presence of input and showed significant phenotypic switching to the “chaste” fate as is observed for the ON state control.

The molecular network diverters composed with the pHIGH-*Msg5* promoter-regulator pair highlight key design considerations associated with tuning network diverters to cross the associated transitory range to alternative phenotypes. The pathway response curve requires switches with stringent control over basal expression levels to maintain quiescence in the absence of the environmental trigger. While switch S4 shows a larger SAR value than S1 and S2 (Supplementary Figure 2.3A), the basal expression level from the diverter incorporating S4 inhibited pathway signaling sufficiently to eliminate cell cycle arrest in the presence of pheromone even in the absence of the input signal, yielding a low PAR value (Figure 2.11). In contrast, switches S1 and S2 exhibit a more stringent control profile than that of S4, and diverters incorporating these switches exhibit larger PAR values and achieve rerouting of cell fate in response to the input

signal. The results highlight the importance of tunable controllers, including those exhibiting stringent profiles, in targeting thresholds of key pathway components to achieve desired phenotypic switching.

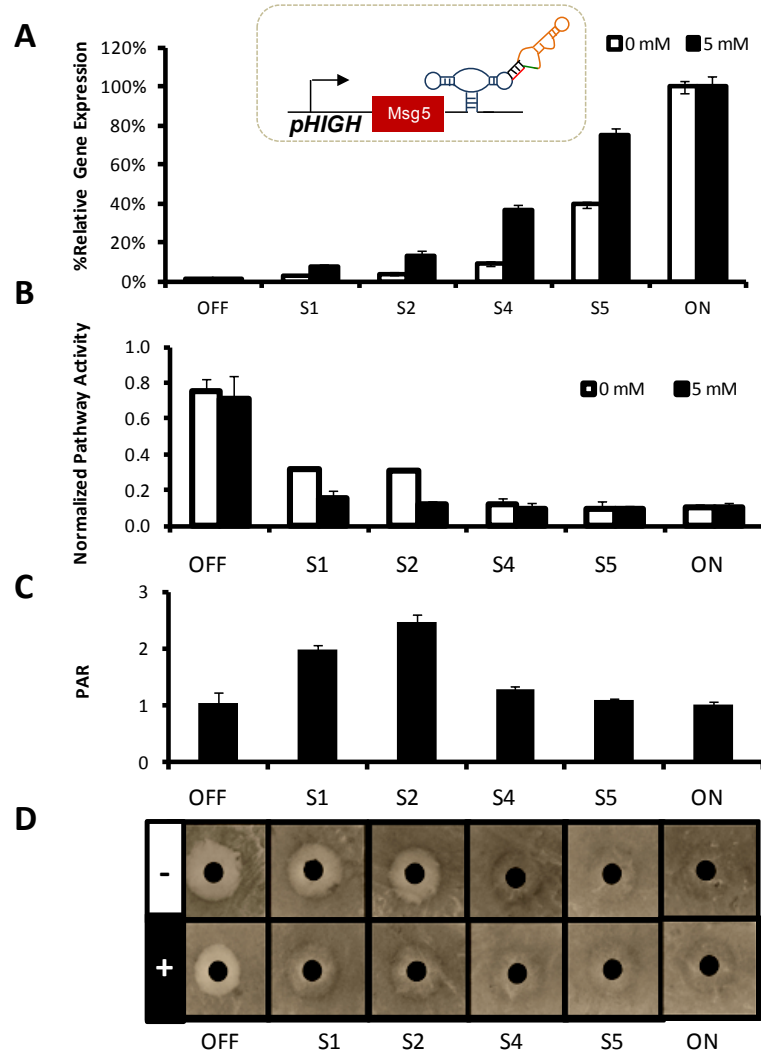


Figure 2.11. Theophylline-inducible molecular network diverters constructed with constitutive *Msg5* expression conditionally route cells to the chaste phenotype. **A.** and **B.** Pairing theophylline-inducible switches of increasing strength from S1 to S4 with constitutive expression of *Msg5* results in decreasing levels of pathway activity. **C.** Addition of theophylline reduces pathway activity most significantly for S1 and S2 as indicated by the higher PAR values. **D.** For S1 and S2, plate assays in the absence of tetracycline show a wild-type halo, while at 5 mM theophylline cells adopt the chaste phenotype.

Negative feedback loops have been shown to reduce population heterogeneity [22]. We examined whether improved fate routing could be achieved by integrating a

feedback architecture with the negative molecular network diverters. The negative feedback diverters were composed by pairing the pFUS1-*Msg5* cassette with various theophylline-responsive switches (Figure 2.12). The low expression level of *Msg5* associated with the feedback diverter incorporating the OFF state control allowed pathway activation in the presence of the pheromone, leading to high GFP levels and wild-type halo formation (Figure 2.12B, D). In contrast, the high expression level of *Msg5* associated from the feedback diverter incorporating the ON state control inhibited pheromone-induced pathway activation, thereby eliminating cell cycle arrest and resulting in low GFP levels. Cell fate diverged from the wild-type to chaste phenotype between S2 and S4. The entire set of feedback diverters showed low PAR values, indicating a weak ability to route from wild-type to chaste fate (Figure 2.12C). Weak phenotypic switching from the negative feedback diverters incorporating switches S1 and S2 was confirmed by plate assays (Figure 2.12D). Diverters incorporating negative feedback may linearize the pathway response curve to *Msg5* expression. As a result of this linearization, changes in *Msg5* expression may be transduced into smaller changes in pathway activity, thus preventing phenotypic switching.

The feedback diverters did not inhibit pathway activation as greatly as the nonfeedback molecular diverters (as measured by transcriptional activation); however, the more active molecular diverters effectively prevented halo formation in the plate assays. Comparing the histograms for the ON and OFF state controls, we observe that while both expression modes reduce the mean of the high GFP population (and thus reduce the level of pathway activation), constitutive expression results in the establishment of a second low GFP population (Supplementary Figure 2.8A, B). GFP

histograms and calculated mean values of the high GFP populations are comparable between the two expression modes (Supplementary Figure 2.8C, D and Supplementary Figure 2.9). These results suggest that cell fate switching at the population level occurs when the mean pathway activity of the high population crosses the critical threshold.

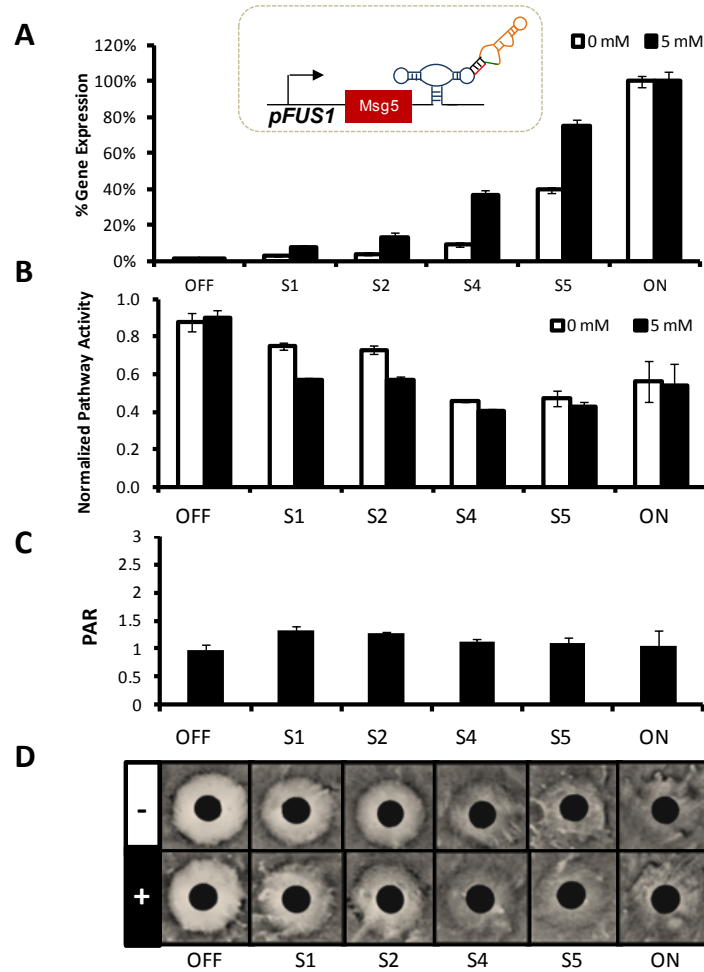


Figure 2.12. Theophylline-inducible molecular network diverters constructed with feedback expression of *Msg5* route cells to the chaste phenotype. A. Pairing theophylline-inducible switches of increasing strength from S1 to S5. **B.** Constructing a negative feedback loop with *Msg5* results in reduced pathway activity across the increasing switch range. **C.** PAR values are noticeably low compared to constitutive expression of *Msg5* (Figure 2.11) **D.** Above S2, cells adopt the chaste phenotype. Only mild phenotypic switching is observed in S1 and S2.

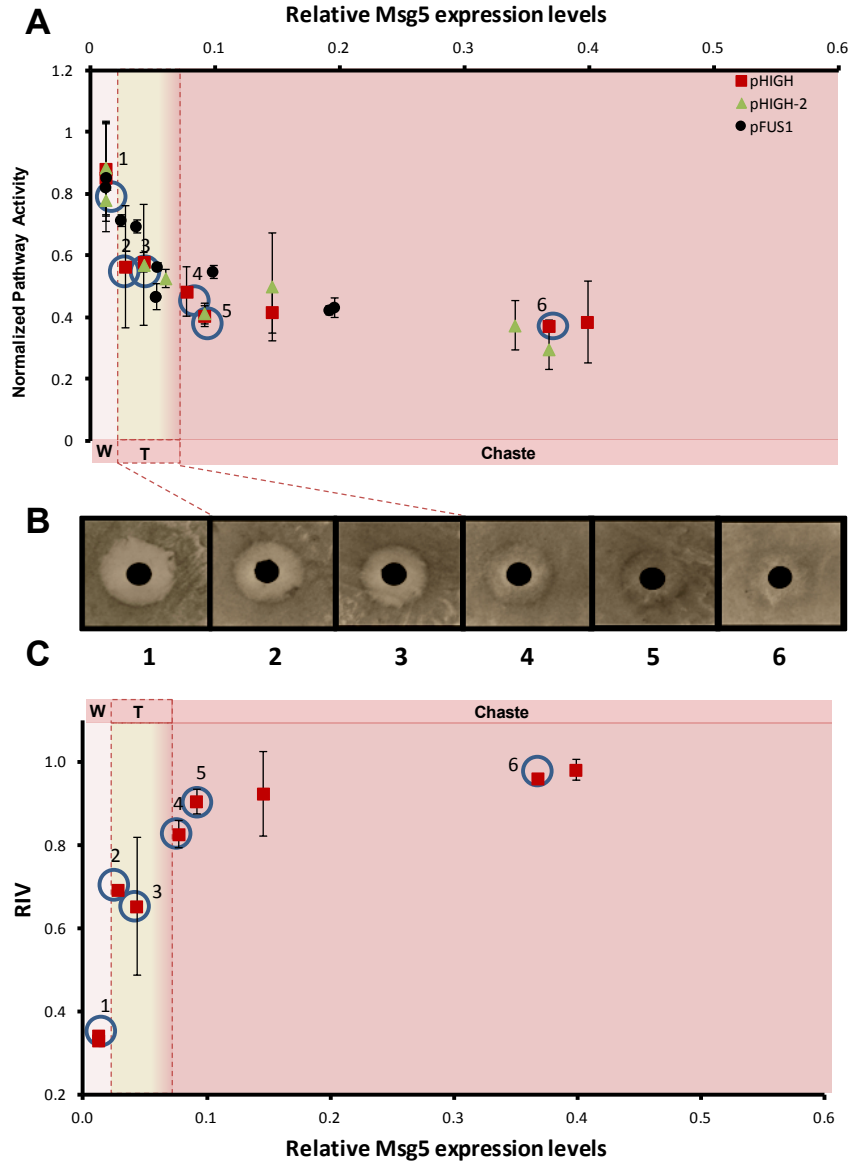


Figure 2.13. Tracing pathway response to *Msg5* expression to the chaste fate. **A.** Pathway activity significantly decreases over a narrow window of relative *Msg5* expression (0 – 0.1). **B.** Above 0.08 expression cells adopt the chaste fate. Plate data correspond to points with numbered circles in **A** selected from the pHIGH-SX data set (Figure 2.11). Relative *Msg5* expression was calculated as described previously. **C.** Relative intensity values (RIV) for constitutive expression of *Msg5* show two regimes of behavior. At low *Msg5* expression (0 – 0.1 relative *Msg5* expression levels), RIV values are increase in a graded response, but above a threshold of *Msg5* cells plateau to high RIV values (above 0.1). High RIV values indicate the difference between inner and outer cell growth as measure by intensity is low. Low RIV values indicate a large difference between inner and outer intensity values (see Methods for calculation of RIV). “W” indicates wild-type. “T” indicates transitory regime.

We used the calculated values of *Msg5* expression to plot the pathway activation curve as described for the positive network diverter. At low *Msg5* levels, a steady

decrease in pathway activity is observed with increasing *Msg5* (Figure 2.13). Within a narrow range of expression the response curve is very sensitive to changes in *Msg5* expression, supporting the observed requirement for switches with stringent control over basal levels to build negative diverters that achieve conditional rerouting of cell fate. To facilitate comparison between both expression modes, pathway activity values were calculated based on the high GFP population. Inclusion of the low GFP population showed similar results for the transitory range and pathway response curve sensitivity (Supplementary Figure 2.10). While we suspect that the pathway response curve for diverters incorporating constitutive expression is more sensitive to changes in *Msg5* than that for feedback diverters, the data do not provide sufficient resolution for differentiating features of the curves that may vary between the two expression modes.

We have demonstrated that negative molecular network diverters can conditionally attenuate pathway activity in the yeast mating pathway, routing cells to the chaste fate. Extending the construction of negative diverters to mammalian cells offers the potential to intervene in the establishment and proliferation of cancers by counteracting aberrant pathway activation. Applying these circuits to diseases such as cancer may reduce or eliminate the proliferation of tumors by checking uncontrolled growth. Additionally, a negative molecular network diverter may be able to restrict pathway attenuation based on temporal and spatial distribution of the environmental trigger limiting the potential side-effects associated with applying such diverters as therapeutics.

Discussion

We have demonstrated the construction of molecular network diverters that positively and negatively regulate pathway activity, conditionally routing cells to alternative fates in response to specific molecular inputs. To construct these diverters, we identified titratable regulators of pathway activity and traced the pathway response curve to regulator levels, identifying the transitory range between the wild-type and alternative fates. In exploring different network architectures, we demonstrated that positive feedback diverters enhance ultrasensitivity in the native pathway, shifting the transitory range for Ste4 to lower levels and providing more robust phenotypic switching. The potency of the negative regulator Msg5 required stringent control of the basal levels for maintenance of the wild-type phenotype in the absence of the environmental trigger. Our studies also demonstrated that these synthetic circuits can be rationally tuned by the exchange of well-characterized genetic parts.

We have demonstrated that within multiple yeast MAPK pathways there are titratable regulators of pathway activity. Ectopic overexpression of specific pathway regulators at these regulatory nodes can be used to modulate pathway activity, providing a readily implementable, modular interface between synthetic regulatory systems and these native pathways. The identification of titratable regulators in multiple pathways suggests that our method for identifying regulators of pathway activity may be broadly applicable to MAPK pathways, facilitating the construction of synthetic circuits that interface with and modulate the function of an important class of signaling pathways. While previous work supports the identified components as regulators of pathway activity [10, 14, 17], we demonstrate that within the mating pathway overexpression of

these regulators above a particular threshold can route to an alternative fate. Additionally, by tracing the pathway response curve in our studies, we have identified the range of regulator expression over which fate transitions from wild-type to the programmed alternative fate. Interestingly, we observed that the transition is reached at lower expression levels for Msg5 than for Ste4, indicating that Msg5 is a more potent regulator of pathway activity. Since Ste4 overexpression leads to cell-cycle arrest, weaker potency of this regulator may represent a control scheme to compensate for variable expression that might otherwise decrease population fitness by reducing overall growth rates. Since Msg5 does not inhibit growth, limiting its potency may be less critical to population fitness.

The pathway response curve is unique to its regulator and dependent on the molecular details of the regulator's interaction with other components in the native network. While modifying the regulator's interaction via protein engineering can change these interactions to reshape the pathway response [8, 17], changing the connectivity of a synthetic circuit can provide a simpler method for rationally reshaping the pathway response curve. In our system, we demonstrated that the introduction of positive feedback shifts the threshold at which cell fate diverges to lower relative Ste4 expression levels, improving phenotypic switching and suggesting an enhancement of the pathway's ultrasensitivity. Further, positive autoregulatory loops such as these have been shown to exhibit bistability [8, 21]. When properly tuned, positive feedback loops can thus provide a providing a type of memory to fate commitment by sustaining the network response when triggered above a particular input level [23]. While the introduction of positive feedback amplifies phenotypic switching from the network diverter, negative feedback

plays a role in reducing population heterogeneity. In our system we observed that the introduction of negative feedback into the network diverter reduced population heterogeneity, resulting in a single narrow peak of pathway activity values. Feedback expression provides a negative response that is proportional to pathway activity which may asymptote to a particular stable state. Mismatches in pathway activity and *Msg5* expression distributions are attenuated for feedback expression. In contrast, constitutive expression results in a more broadly distributed response in which mismatches in pathway expression and regulator expression levels introduced by extrinsic noise increase population heterogeneity. Thus, the introduction of feedback architectures into the molecular network diverters result in synthetic circuits that exhibit useful properties for robust circuit performance, including enhanced ultrasensitivity and reduced population heterogeneity.

We also demonstrate that molecular network diverters can be rationally tuned by the exchange of well-defined genetic parts. Specifically, the promoter and switch elements can be exchanged within the diverter architecture to predictably tune pathway activity. In addition, we showed that the ability of the switch component within the diverter to route cell fate is independent of the input signal the switch is programmed to detect and dependent on the quantitative gene-regulatory activities exhibited by the switch. This property allows for orthogonal sets of network diverters, which can be triggered by independent input channels, to be designed through the incorporation of RNA switches responsive to different molecular inputs. Further, independent channels of regulation provide for the integration of multiple network diverters that control different pathway nodes, allowing independent triggering of each diverter. This capability can

ultimately be used to route genetically identical cells to different cell fates dependent on the small-molecule trigger present in the environment. Such orthogonal control strategies may facilitate patterning of multiple cell fates from a genetically homogenous culture via the controlled distribution of small-molecule triggers.

Our studies also highlight the design trade-offs and considerations in configuring network diverters to span the range of expression required for fate routing. While RNA switches with higher SAR values exhibit greater fold changes in regulator expression, regulators that exhibit high activities, such as *Msg5*, require more stringent switches with lower basal levels that can exhibit smaller dynamic ranges (SAR). In certain situations, the optimal diverter configuration and fate switching may not be achievable based on the pathway response curve and the set of available parts for composing the diverter. Therefore, the development of strategies to amplify input-triggered switching and an expanded the set of switches (and corresponding range of properties) will extend the number of native pathways to which molecular network diverters can be applied. In addition, the switch component provides a promoter-independent strategy for tuning gene expression, potentially providing greater flexibility to the control system, particularly in situations in which the application constrains the choice of promoter. For example, synthetic systems developed as therapies for the treatment of diabetes and gout require specific pathway-responsive promoters [24, 25]. In addition to facilitating tuning in these synthetic systems, the RNA switches will enable the construction of synthetic networks that provide exogenous spatial and temporal regulation, providing a strategy for limiting the extent of side-effects associated with such therapies.

The molecular network diverter architecture developed in this study offers the potential to independently trigger a positive and negative diverter via independent small-molecule input channels, allowing routing to three different fates from a genetically identical cell population. However, the integration of both positive and negative diverters into a single cell poses challenges in maintaining the performance of each diverter. While each diverter runs quiescently with respect to fate routing in the absence of small-molecule input, addition of the diverter measurably changes the basal activity of the pathway. Since the opposing diverters perform opposite functions on pathway activity that are processed through the native network, basal expression levels from the non-triggered diverter may antagonize routing from the triggered diverter. The incorporation of RNA switches exhibiting low basal levels and large dynamic ranges may facilitate improved routing in such system designs. However, computational models of RNA switches have indicated a tradeoff in tuning the stringency of a switch and its sensitivity to the input ligand, ultimately impacting the dynamic range [26]. Network architectures that amplify small-molecule triggered routing may enhance fate switching even in the presence of diverter antagonization. Issues with basal expression levels impinging on circuit performance have been observed in synthetic network construction [23, 27, 28]. Researchers have addressed such issues by adding layers of post-transcriptional control, such as through riboregulators in bacteria [29] and microRNAs in mammalian cells [30, 31], to reduce gene expression leakage in the OFF state. Thus, RNA control elements that target the opposite regulator may be coexpressed with pathway regulators or imbedded within the opposite transcript to achieve reduced basal level leakage, diminished diverter

antagonization, and amplified diverter-mediated switching when positive and negative diverters are simultaneously implemented.

While our work elucidates the design principles for constructing molecular network diverter systems in yeast, these principles can be extended to construct similar systems in higher eukaryotes, offering the potential to probe native networks in multicellular organisms, program tissue formation, and target cancer therapies with synthetic molecular network diverters. Additionally, these synthetic circuits may provide the control tools necessary for the *ex vivo* construction of complex tissues when combined with designer scaffolds printed with small-molecule triggers. Further, our work highlights the utility of control systems that can be conditionally induced while maintaining endogenous connectivity with independent promoter selection. For genetic programs that decrease fitness or viability, such systems allow for conditional induction at the appropriate time, reducing the selection pressure to eliminate the prescribed program. As RNA switches are generated to sense a broader array of molecular ligands, diverters may be configured to respond to endogenous inputs, potentially allowing autonomous control within the cell. As our ability to build interfaces between synthetic circuits and native networks improves, synthetic biological devices that control cell fate will translate into therapeutic and regenerative medicine applications, as well as facilitate the study of natural biological systems.

Materials and methods

Plasmid and strain construction

Standard molecular biology cloning techniques were used to construct all plasmids [32]. DNA synthesis was performed by Integrated DNA Technologies (Coralville, IA). All enzymes, including restriction enzymes and ligases, were obtained through New England Biolabs (Ipswich, MA). Ligation products were electroporated with a GenePulser XCell (Bio-Rad, Hercules, CA) into an *E. coli* DH10B strain (Invitrogen, Carlsbad, CA), where cells harboring cloned plasmids were maintained in Luria-Bertani media containing 50 mg/ml ampicillin (EMD Chemicals). All cloned constructs were sequence verified by Laragen Inc (Santa Monica, CA).

Plasmids expressing GFP were constructed from pCS321 (Supplementary Figure 2.11A, Supplementary Table 2.1 [33]. Promoters pLOW (pADH1), pMED (pCYC1), pHIGH (TEF1 mutant 7) [34], pHIGHEST (pTEF1), pSTL1, and pFUS1 were PCR amplified and cloned into SacI (or NotI) and BamHI in pCS321 using promoter-specific primers (Supplementary Table 2.2).

Plasmids for galactose-titration were constructed from pCS1128 a TRP plasmid which bears pGAL1-yEGFP-CYCt with an ON state control cloned in the 3'UTR between AvrII and XhoI (Supplementary Figure 2.11B, Supplementary Table 2.3). Mating genes (Ste4, Ste50, Ste11, Ste7, Fus3, Msg5) and osmo genes (Pbs2, Hog1, Ptc1) were cloned between AvrII and BamHI using gene-specific primers for amplification from plasmid and genomic templates (Supplementary Table 2.2). XhoI restriction sites in Fus3 and Ste4 and an AvrII restriction site in Ste7 were removed by site-directed mutagenesis using QuikChange II Site-directed mutagenesis kit (Agilent, Santa Clara,

CA) according to the manufacturer's instruction with appropriate primers (Supplementary Table 2.4). Pbs2 was cloned into pCS321 using the same primers and restriction sites to generate a URA plasmid Pbs2 titration construct.

To construct the negative and positive molecular network diverters, Msg5 and Ste4 were cloned into the GFP expressing constructs with the various promoters as described above for the galactose titration constructs. Ribozyme-based devices and appropriate controls (Supplementary Table 2.5) were inserted into the 3' UTR via the unique restriction sites AvrII and XhoI, located immediately downstream of the gene stop codon as described previously (Supplementary Tables 3.6 and 3.7) [33].

Reporter strains for galactose-titration studies were constructed by knocking out the galactose transporter, GAL2, to construct the mating strain CSY532 and osmolarity strain CSY139. The pFUS1-yEGFP3-CYC1t cassette from pCS1124 was cloned into pCS1391, a loxP integrating vector [35], via the unique restriction sites SacI and KpnI to make pCS2292 (Supplementary Figure 2.12, Supplementary Table 2.8). pFUS1-yEGFP3-CYC1t was chromosomally integrated into yeast strain CSY364 (EY1119; W303a Δ sst1 Δ kss1::HIS3) [36] via homologous recombination using the gene cassette from pCS2292 to construct yeast strain CSY532 (W303a Δ sst1 Δ kss1::HIS3 gal2 ::FUS1p-yEGFP3-loxP-KanR) (Supplementary Table 2.9). Briefly, the pFUS1-yEGFP3-loxP-KanR cassette was PCR amplified using Expand High Fidelity PCR system (Roche, Indianapolis, IN) from pCS2292 using forward and reverse primers (Supplementary Table 2.10), each carrying 60 nts of homologous sequence to the *GAL2* locus. Yeast strain EY1119 was transformed with 12 μ g of gel purified PCR product and plated on G418 plates to build yeast strain CSY532. CSY408 was constructed as described above using a blank

integration cassette. To construct a reporter for the osmolarity pathway, pSTL1-yEGFP-CYC1t was cloned into a yeast disintegrator plasmid pCS1441 which is specific to the FCY1 locus via unique restriction site KpnI and SacI. CSY408 was transformed with disintegrator vector bearing pSTL1-yEGFP-CYC1t linearized by digestion with AscI as described previously [37] to yield KGY139. For characterization of the molecular network diverters, yeast strain CSY840 was constructed as described for CSY532 using primers specific to the *TRP1* locus (Supplementary Tables 3.9 and 3.10).

Measuring mating pathway activity via a transcriptional reporter

For the galactose titration studies, plasmids bearing the galactose-inducible promoter (pGAL1) controlling expression of various pathway regulators and appropriate controls were transformed into yeast strain CSY532. Cells were inoculated into the appropriate dropout media, grown overnight at 30°C, and back diluted into fresh media in the presence of varying concentrations of galactose (0, 0.25, 0.5, 1, 2 and 3%) to an OD₆₀₀ of < 0.1. To identify negative pathway regulators, after growing for 3 hr at 30°C, cells were stimulated with saturating pheromone levels, to a final concentration of 100 nM α mating factor acetate salt (Sigma-Aldrich, St. Louis, MO), to activate the mating pathway. The pathway was not stimulated when evaluating the potential of positive regulators. Following 6 hr of growth post-back-dilution, GFP fluorescence levels from the pFUS1-yEGFP3 reporter were evaluated via flow cytometry using a Cell Lab Quanta SC flow cytometer (Beckman Coulter, Fullerton, CA) with the following settings: 488-nm laser line, 525-nm bandpass filter, and photomultiplier tube setting of 5.0 on FL1 (GFP). Fluorescence data were collected under low flow rates for ~ 10,000 viable cells.

Normalized pathway activity is calculated as the geometric mean of three biological replicates of each sample normalized to the blank plasmid control not bearing a gene at the corresponding galactose concentration.

The molecular diverter plasmids and appropriate controls were transformed into yeast strain CSY840. Cells were inoculated into the appropriate drop-out media, grown overnight at 30°C, and back diluted into fresh media in the presence or absence of ligand at the specified concentration to an OD₆₀₀ of < 0.1. For negative diverters, after growing for 3 hr at 30°C, cells were stimulated with saturating pheromone levels, to a final concentration of 100 nM α mating factor acetate salt, to activate the mating pathway. Following 6 hr of growth post-back-dilution, GFP fluorescence levels from the pFUS1-yEGFP3 reporter were evaluated via flow cytometry using a Cell Lab Quanta SC flow cytometer as described previously. Normalized pathway activity is calculated as the geometric mean of three biological replicates of each sample normalized to the blank plasmid control stimulated with saturating α mating factor in the absence of either small molecule.

Measuring osmolarity pathway activity via a transcriptional reporter

Galactose titration studies in the osmolarity pathway were performed as described previously for the mating pathway with the following exceptions. Cells were transformed in KGY139 to measure the activity of the osmolarity pathway via the integrated pSTL1-GFP reporter. Normalized pathway activity is calculated relative to the pathway stimulated with 1M sorbitol for 6 hr. Quanta flow cytometer photomultiplier tube setting of 7.5 on FL1 (GFP).

Measuring mating pathway activity via halo assays

Mating associated cell-cycle arrest was evaluated via halo assays [38]. Halo assays were performed on cultures grown overnight in YNB with appropriate dropout solution, back diluted into fresh media, and grown to $OD_{600} \sim 0.2\text{--}0.4$. 200 μl of each replicate was plated on the appropriate drop-out plates. For galactose-titration halo assays, cells were plated on noninducing, nonrepressing plates with varying concentrations of galactose (0, 0.25, 0.5, 1, 2 and 3%). For characterization of the molecular network diverters, cells were plated on plates containing no small molecule or 5 mM theophylline or 1 mM Tetracycline as specified. After plating the cells, a gradient of α mating factor was established by saturating a filter disk (2 mm diameter) of Whatman paper with 9 μl of 0.1 mg/mL α mating factor and placing the disk on the center of the plate. Cells were grown for 18 hr at 30°C and imaged via epi-white illumination with a GelDoc XR+ System (Bio-Rad).

Relative intensity values (RIV) were calculated to measure the difference in inner and outer halo cell growth. Intensity of rectangular cross-sections at $r = 0.15$ inches (inner region) and $r = 0.5$ inches (outer region) from the filter disc were calculated using image processing software from the GelDoc XR+ System. The difference between outer and inner intensity values were calculated for each plate to yield the plate's intensity range. The difference between each plate intensity range and max intensity range was calculated and normalized by the max intensity range. The max intensity range was calculated by subtracting the minimal intensity value from the maximal intensity value for the entire set

of plates including both nonswitch controls and the blank plasmid control. Increasing RIV values indicate decreasing differences in inner and outer intensities.

Measuring mating pathway activity via Western blots

Yeast cells harboring appropriate constructs were grown as indicated above in 5 mL cultures to ~ 1.0 OD₆₀₀, pelleted via centrifugation, and resuspended in 800 μ L modified RIPA Lysis buffer (50 mM Tris-HCl (pH 7.5), 150 mM NaCl, 1% Triton X-100, 0.5% Nonidet P-40, 0.25% sodium deoxycholate, 50 mM β -glycerophosphate (pH 7.3), 10 mM NaPP, 30 mM NaF, 1 mM benzamidine, 2 mM EGTA, 1 mM sodium orthovanadate, 1 mM dithiothreitol, 5 μ g/ml aprotinin, 5 μ g/ml leupeptin, 1 μ g/ml pepstatin and 1 mM phenylmethylsulfonyl fluoride). The resuspended cell mixture was added to a tube containing 1 mm glass beads and shaken for 5 min at 30/sec in a homogenizer to generate cell lysates. Following homogenization, the lysates were boiled for 5 minutes in a 95 °C sand bath and subsequently centrifuged at maximum speed for 2 min. The supernatant was recovered into a fresh tube. Cleared lysates were stored at -80°C.

Sample analysis was performed by adding one part 10X SDS sample buffer (50 mM Tris-HCl (pH=6.8), 12% (vol/vol) glycerol, 2% (wt g/vol ml) SDS, 1% DTT, 0.01% (wt g/vol ml) bromophenol blue) to 9 parts of the cell lysate. Samples were heated at 100°C for 5 min and subsequently loaded on a 10% acrylamide SDS-polyacrylamide gel. 3 μ L of SeeBlue Plus2 Prestained Standard (Invitrogen) was loaded into a separate lane as a size marker. Different volumes of lysate and loading buffer were added to each lane up to a total volume of 30 μ L to adjust for equal protein loading. The gel was run at 50

mA for ~ 1 hr and transferred in transfer buffer and apparatus to nitrocellulose. Immunoblotting and imaging was performed as previously described using an anti-phospho P44/42 antibody (Cell Signaling Technology to detect phosphorylated Fus3 and anti-Cdc28 as a loading control (Sc-53, Santa Cruz Biotechnology, Inc, Santa Cruz, CA) [39].

Calculating relative Ste4 and Msg5 expression levels

For constitutive expression of Ste4 and Msg5, each construct's promoter strength (Supplementary Figure 2.2) was multiplied by the switch percent expression at the appropriate ligand concentration. Each value was normalized to expression calculated from pHIGH-ON (the highest expression in these assays). For feedback expression, normalized pathway activity values (pFUS1-GFP) were taken as a proxy for the strength of pFUS1-Ste4 or pFUS1-Msg5 expression. These values were evaluated as a measure the promoter strength and, as for constitutive expression, multiplied by the switch percent expression at the appropriate ligand concentration. Each value was normalized to expression calculated from pHIGH-ON.

Acknowledgements

Special thanks to Richard Yu for technical advice for halo assays, Stephen Chapman for technical assistance with mating assays and Western blots, and the Van Drogen lab for constructs. Funding provided by the National Institutes of Health (R01GM086663).

References

1. Seger R, Krebs EG: **The MAPK signaling cascade.** *Faseb J* 1995, **9**:726-735.
2. Hanahan D, Weinberg RA: **The hallmarks of cancer.** *Cell* 2000, **100**:57-70.
3. McCormick F: **Signalling networks that cause cancer.** *Trends Cell Biol* 1999, **9**:M53-56.
4. Discher DE, Mooney DJ, Zandstra PW: **Growth factors, matrices, and forces combine and control stem cells.** *Science* 2009, **324**:1673-1677.
5. Lutolf MP, Gilbert PM, Blau HM: **Designing materials to direct stem-cell fate.** *Nature* 2009, **462**:433-441.
6. Chapman S, Asthagiri AR: **Resistance to signal activation governs design features of the MAP kinase signaling module.** *Biotechnol Bioeng* 2004, **85**:311-322.
7. Levchenko A, Bruck J, Sternberg PW: **Scaffold proteins may biphasically affect the levels of mitogen-activated protein kinase signaling and reduce its threshold properties.** *Proc Natl Acad Sci U S A* 2000, **97**:5818-5823.
8. Wang X, Hao N, Dohlman HG, Elston TC: **Bistability, stochasticity, and oscillations in the mitogen-activated protein kinase cascade.** *Biophys J* 2006, **90**:1961-1978.
9. Andersson J, Simpson DM, Qi M, Wang Y, Elion EA: **Differential input by Ste5 scaffold and Msg5 phosphatase route a MAPK cascade to multiple outcomes.** *Embo J* 2004, **23**:2564-2576.
10. Ingolia NT, Murray AW: **Positive-feedback loops as a flexible biological module.** *Curr Biol* 2007, **17**:668-677.

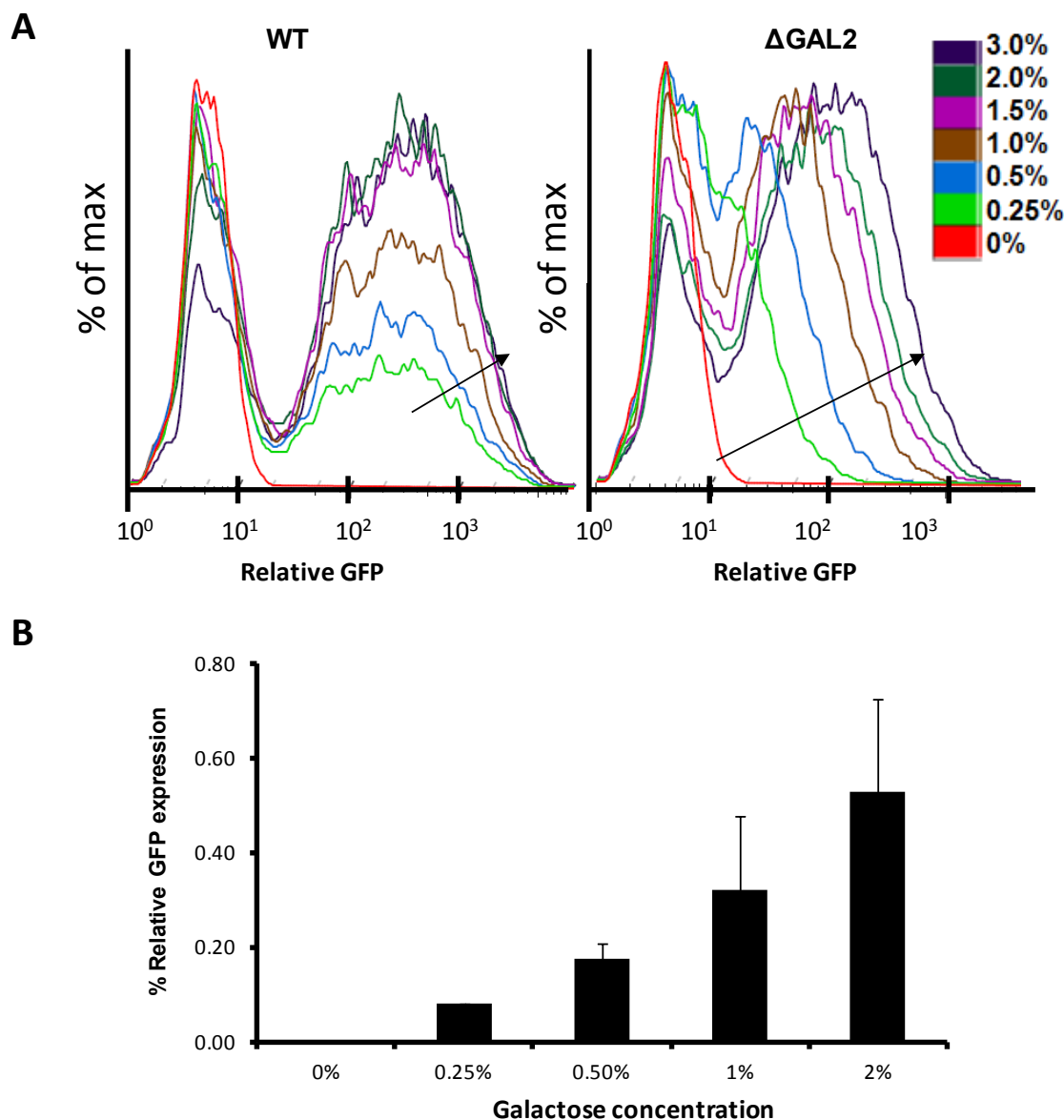
11. Santos SD, Verveer PJ, Bastiaens PI: **Growth factor-induced MAPK network topology shapes Erk response determining PC-12 cell fate.** *Nat Cell Biol* 2007, **9**:324-330.
12. Win MN, Smolke CD: **A modular and extensible RNA-based gene-regulatory platform for engineering cellular function.** *Proc Natl Acad Sci U S A* 2007.
13. Palpant RG, Steimnitz R, Bornemann TH, Hawkins K: **The Carter Center Mental Health Program: addressing the public health crisis in the field of mental health through policy change and stigma reduction.** *Prev Chronic Dis* 2006, **3**:A62.
14. Bashor CJ, Helman NC, Yan S, Lim WA: **Using engineered scaffold interactions to reshape MAP kinase pathway signaling dynamics.** *Science* 2008, **319**:1539-1543.
15. Varghese J, Cohen SM: **microRNA miR-14 acts to modulate a positive autoregulatory loop controlling steroid hormone signaling in Drosophila.** *Genes Dev* 2007, **21**:2277-2282.
16. Herranz H, Cohen SM: **MicroRNAs and gene regulatory networks: managing the impact of noise in biological systems.** *Genes Dev* 2010, **24**:1339-1344.
17. Park SH, Zarrinpar A, Lim WA: **Rewiring MAP kinase pathways using alternative scaffold assembly mechanisms.** *Science* 2003, **299**:1061-1064.
18. Mettetal JT, Muzzey D, Gomez-Uribe C, van Oudenaarden A: **The frequency dependence of osmo-adaptation in Saccharomyces cerevisiae.** *Science* 2008, **319**:482-484.

19. Nevozhay D, Adams RM, Murphy KF, Josic K, Balazsi G: **Negative autoregulation linearizes the dose-response and suppresses the heterogeneity of gene expression.** *Proc Natl Acad Sci U S A* 2009, **106**:5123-5128.
20. Xiong W, Ferrell JE, Jr.: **A positive-feedback-based bistable 'memory module' that governs a cell fate decision.** *Nature* 2003, **426**:460-465.
21. Ferrell JE, Jr.: **Self-perpetuating states in signal transduction: positive feedback, double-negative feedback and bistability.** *Curr Opin Cell Biol* 2002, **14**:140-148.
22. Becskei A, Serrano L: **Engineering stability in gene networks by autoregulation.** *Nature* 2000, **405**:590-593.
23. Ajo-Franklin CM, Drubin DA, Eskin JA, Gee EP, Landgraf D, Phillips I, Silver PA: **Rational design of memory in eukaryotic cells.** *Genes Dev* 2007, **21**:2271-2276.
24. Han J, McLane B, Kim EH, Yoon JW, Jun HS: **Remission of diabetes by insulin gene therapy using a hepatocyte-specific and glucose-responsive synthetic promoter.** *Mol Ther* 2011, **19**:470-478.
25. Kemmer C, Gitzinger M, Daoud-El Baba M, Djonov V, Stelling J, Fussenegger M: **Self-sufficient control of urate homeostasis in mice by a synthetic circuit.** *Nat Biotechnol* 2010, **28**:355-360.
26. Beisel CL, Smolke CD: **Design principles for riboswitch function.** *PLoS Comput Biol* 2009, **5**:e1000363.
27. Gardner TS, Cantor CR, Collins JJ: **Construction of a genetic toggle switch in *Escherichia coli*.** *Nature* 2000, **403**:339-342.

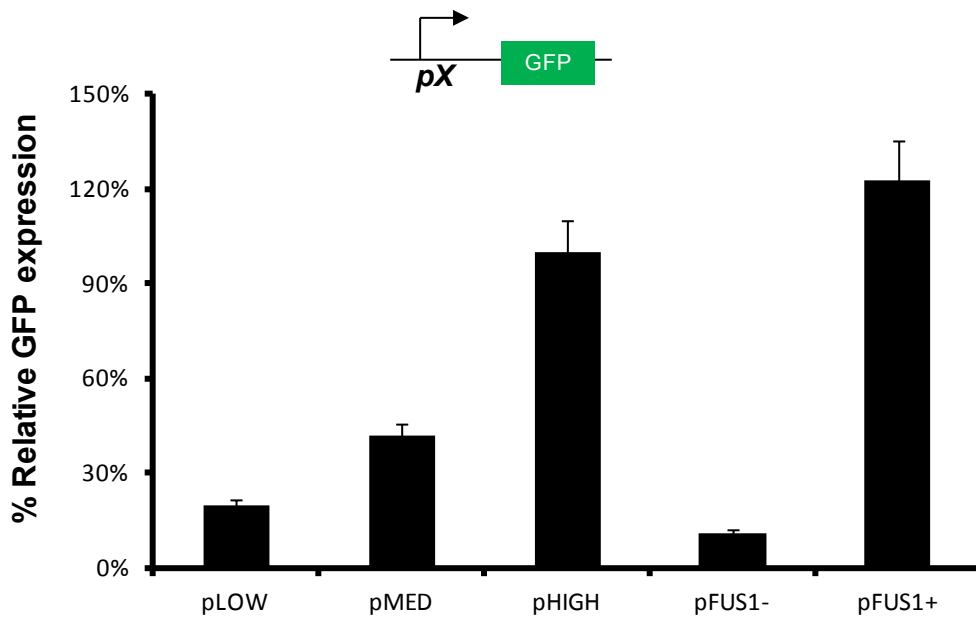
28. Friedland AE, Lu TK, Wang X, Shi D, Church G, Collins JJ: **Synthetic gene networks that count.** *Science* 2009, **324**:1199-1202.
29. Callura JM, Dwyer DJ, Isaacs FJ, Cantor CR, Collins JJ: **Tracking, tuning, and terminating microbial physiology using synthetic riboregulators.** *Proc Natl Acad Sci U S A* 2010, **107**:15898-15903.
30. Deans TL, Cantor CR, Collins JJ: **A tunable genetic switch based on RNAi and repressor proteins for regulating gene expression in mammalian cells.** *Cell* 2007, **130**:363-372.
31. Xie Z, Wroblewska L, Prochazka L, Weiss R, Benenson Y: **Multi-input RNAi-based logic circuit for identification of specific cancer cells.** *Science* 2011, **333**:1307-1311.
32. Sambrook J RD: *Molecular Cloning: A Laboratory Manual, 3rd edn.* Cold Spring Harbor, NY: Cold Spring Harbor Lab Press; 2001.
33. Win MN, Smolke CD: **A modular and extensible RNA-based gene-regulatory platform for engineering cellular function.** *Proceedings of the National Academy of Sciences* 2007, **104**:14283-14288.
34. Nevoigt E, Kohnke J, Fischer CR, Alper H, Stahl U, Stephanopoulos G: **Engineering of promoter replacement cassettes for fine-tuning of gene expression in *Saccharomyces cerevisiae*.** *Appl Environ Microbiol* 2006, **72**:5266-5273.
35. Guldener U, Heck S, Fielder T, Beinhauer J, Hegemann JH: **A new efficient gene disruption cassette for repeated use in budding yeast.** *Nucleic Acids Res* 1996, **24**:2519-2524.

36. Flotho A, Simpson DM, Qi M, Elion EA: **Localized feedback phosphorylation of Ste5p scaffold by associated MAPK cascade.** *J Biol Chem* 2004, **279**:47391-47401.
37. Sadowski I, Su TC, Parent J: **Disintegrator vectors for single-copy yeast chromosomal integration.** *Yeast* 2007, **24**:447-455.
38. Sprague GF, Jr.: **Assay of yeast mating reaction.** *Methods Enzymol* 1991, **194**:77-93.
39. Chapman SA, Asthagiri AR: **Quantitative effect of scaffold abundance on signal propagation.** *Mol Syst Biol* 2009, **5**:313.

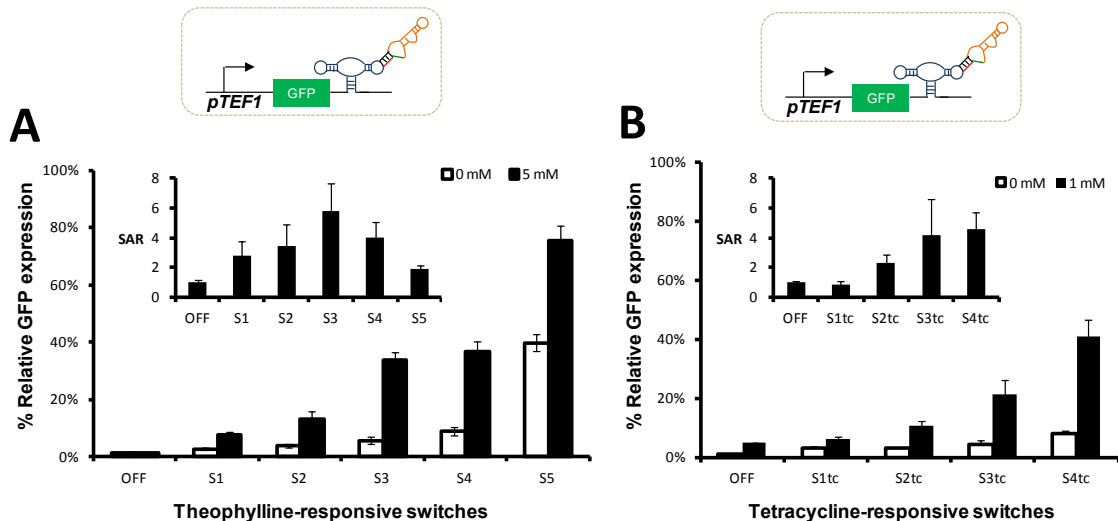
Supplementary figures



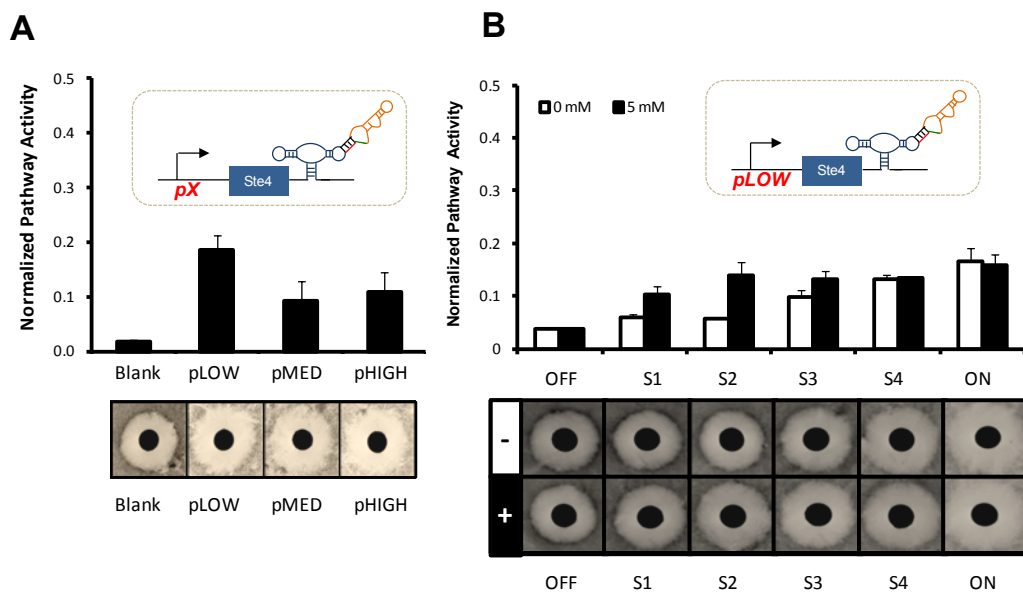
Supplementary Figure 2.1. Engineered strain linearly increases the mean level of expression from the galactose-inducible promoter in response to increasing galactose. A. Histograms for the wild-type (WT) strain show that the mean levels of expression do not significantly change in response to increasing levels of galactose. In the engineered strain (Δ GAL2), histograms demonstrate that the mean fluorescence increases linearly with galactose concentration. In both strains, the percentage of cells in the high expression population increases as galactose levels increase. Arrows indicate direction of increasing galactose concentration. Cellular fluorescence was measured via flow cytometry 6 hours post-induction with galactose from cells harboring a construct bearing pGAL1-Fus3-GFP. Histograms are from single samples and are representative of three replicates. **B.** Mean fluorescence levels of GFP from cells bearing a plasmid with pGAL1-GFP. Assays were performed as described previously. Data represents mean of three replicates with the 0% (noninduced) control subtracted and values normalized to pHIGH-GFP expression levels. Standard deviation is used for the error bars.



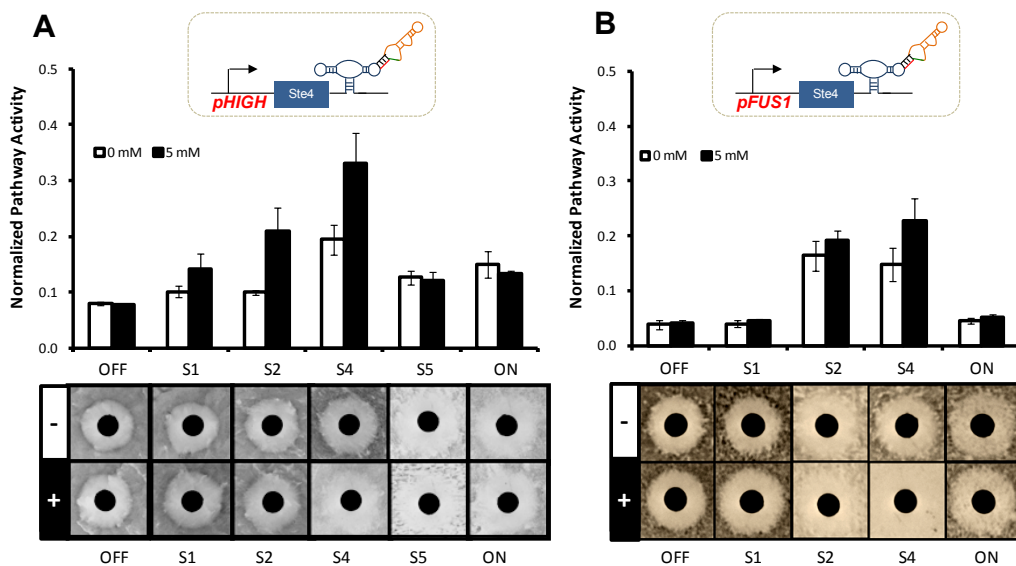
Supplementary Figure 2.2. Promoter characterization. Promoter characterization is critical for placing the regulators at the appropriate levels of expression. Mean values of viable cells were calculated and normalized by the value of pHIGH. Not shown on the graph is pHIGHEST which is more than 6 times higher than pHIGH (reference TEF1 library). pLOW refers to pADH1, pMED to pCYC1, pHIGH to pTEF1mutant7 and pHIGHEST to pTEF1. pFUS1 is the mating-responsive promoter. GFP values were determined in the absence of α factor (pFUS1-) and at saturating concentration (100 nM, pFUS1+) three hours following stimulation.



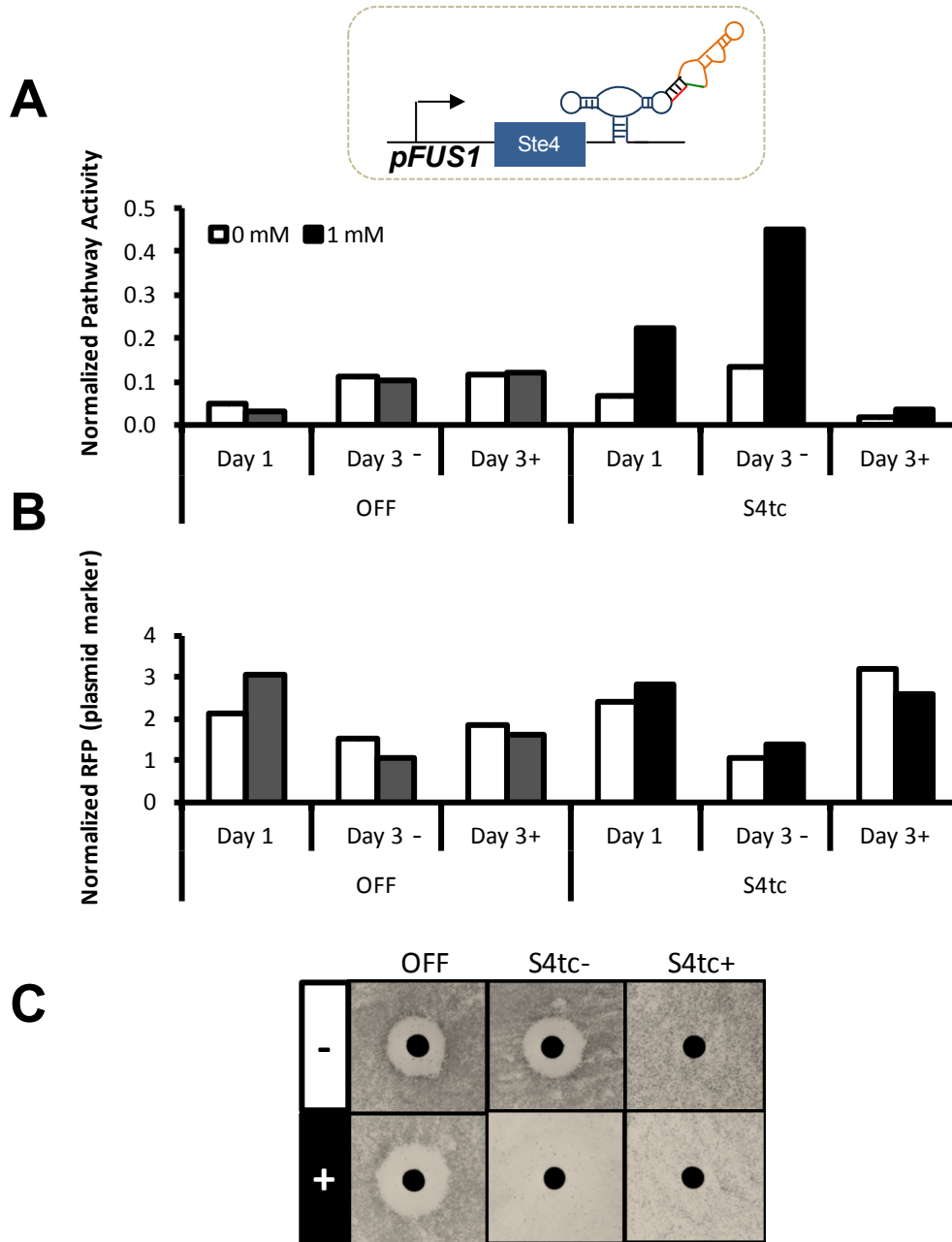
Supplementary Figure 2.3. Range of switch expression strengths. **A.** Theophylline-responsive switches' basal levels, the expression levels in the absence of ligand, range from 3% to 40% of the ON control. S3 has the highest switch activation ratio (SAR) at 5.7. SAR is the ratio of expression levels in the presence of ligand to the level in the absence of ligand. **B.** Tetracycline-responsive switches' basal levels range from 3% to 8%. S3tc and S4tc have similar high SARs at 5.2 and 5.1, respectively.



Supplementary Figure 2.4. Constitutive expression with low-strength promoter shows high pFUS1-GFP levels, yet switches fail to cross the phenotypic transitory range. **A.** Counterintuitively, higher pFUS1-GFP resulted from Ste4 expression from the LOW promoter compared to either the MED or HIGH promoter. Halo assays demonstrated similar phenotypic outcome across the range. **B.** Ste4 expression from the LOW promoter and paired with a range of theophylline-responsive switches shows weak routing to the promiscuous fate. As switch strength increases, cell growth slowly diminishes but ligand-induced routing to the promiscuous fate is not observed. The threshold to the promiscuous fate is postulated to be above the pLOW-Ste4-ON expression levels.

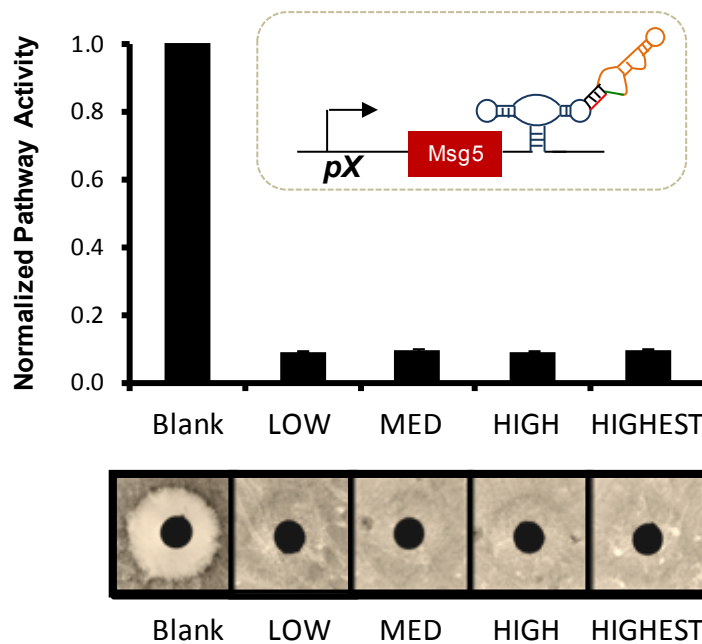


Supplementary Figure 2.5. Theophylline-inducible positive network diverters mirror response of tetracycline-responsive diverters. **A.** Ste4 expression from pHIGH paired with theophylline-responsive switches shows that pathway activity increases across the range up to S4. Above S3 expression levels, pathway activity as measured by pFUS1-GFP drops. Addition of theophylline increases pathway activity for each switch construct up to S3. For S3, plate assays in the absence of theophylline show a wild-type halo, while at 5 mM theophylline cells adopt the promiscuous phenotype. **B.** Constructing a positive feedback loop amplifies ligand-induced phenotype switching. S3 shows theophylline-induced phenotype switching.

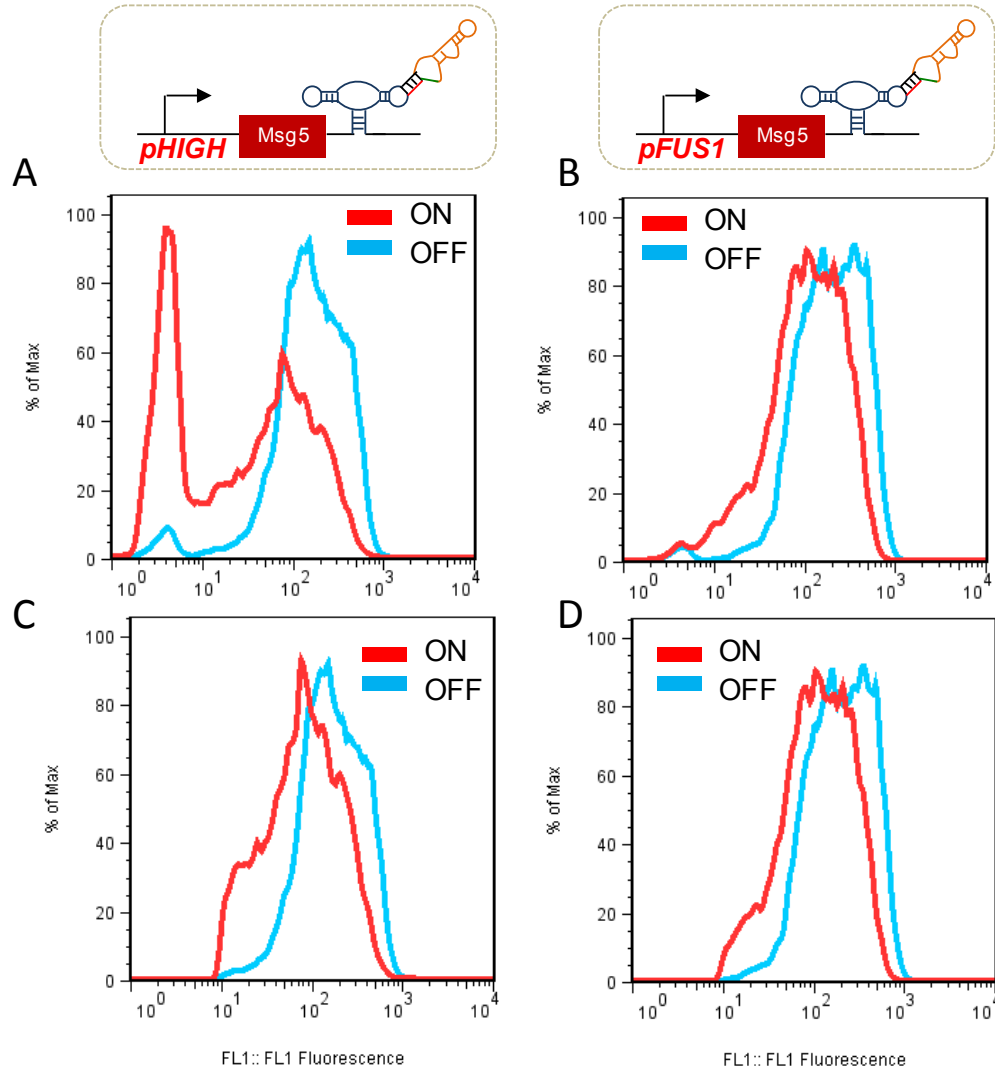


Supplementary Figure 2.6. Selection of mating-resistant cells occurs over time at superthreshold levels of positive feedback. **A.** Pathway activity drops over time for cells grown at super-threshold levels of positive feedback but not at low levels of positive feedback. Cells expressing the OFF state control with pFUS1-Ste4 show constant, low levels of pathway activity whether grown in the presence (+) or absence (-) of tetracycline for 2 days. S4tc shows normal increases in pathway activity when triggered with tetracycline on Day 1 and Day 3. However, cells triggered after 2 days growth in tetracycline, at superthreshold levels of positive feedback, do not significantly upregulate pathway activity. Instead, these cells adopt a low pFUS1-GFP profile. Cells were inoculated overnight and on Day 1 back-diluted into the indicated concentration of tetracycline. After 6 hours, fluorescence values for GFP were measured by flow cytometry as described previously. Cells were grown in the presence (+) or absence (-) of tetracycline another 18 hours before back-dilution on Day 2. Cells were then grown 24 hours, back diluted in the presence or absence of tetracycline. After 6 hours, fluorescence levels were measured. **B.** Constitutively expressed

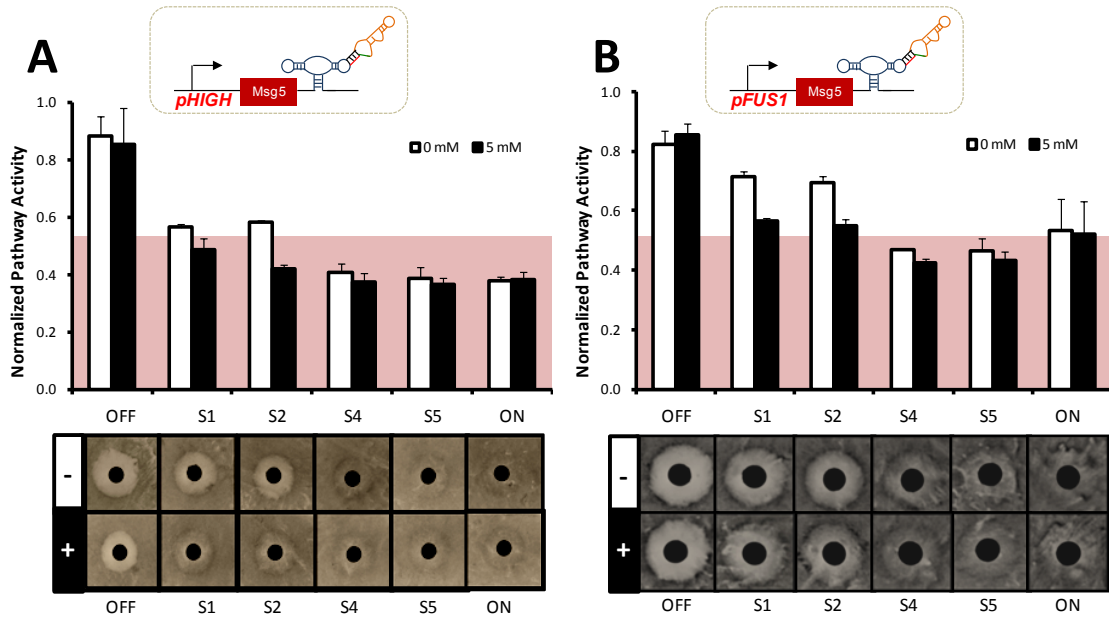
RFP acts as a plasmid marker and indicator of expression from the plasmid. RFP plasmid marker data do not show a correlation between selective pressure and RFP values. Cells experiencing strong selective pressure do not reduce or eliminate expression from the plasmid more than at low selective pressure. These data suggest that mating-resistant cells evade the arrest-inducing program by a method other than jettisoning the plasmid. RFP fluorescence was determined by spectrophotometer plate reader with excitation at 587 nm and emission 610 nm. RFP values were normalized by cells density as measured by absorbance at 600 nm. Final values were computed by dividing by the non-RFP fluorescent control at the corresponding tetracycline concentration. C. Halo assays with cells plated in the presence or absence of 1 mM tetracycline after 3 days of growth. pFUS1-Ste4-S4tc shows that cells maintain routing ability after 3 days when grown in the absence of tetracycline (S4tc-). Cells bearing pFUS1-Ste4-S4tc grown in the presence of tetracycline (S4tc+) show resistance to pheromone-induced cell cycle arrest, but still respond to tetracycline by modestly reducing cell growth. The OFF state control maintains normal halo formation in the presence or absence of tetracycline.



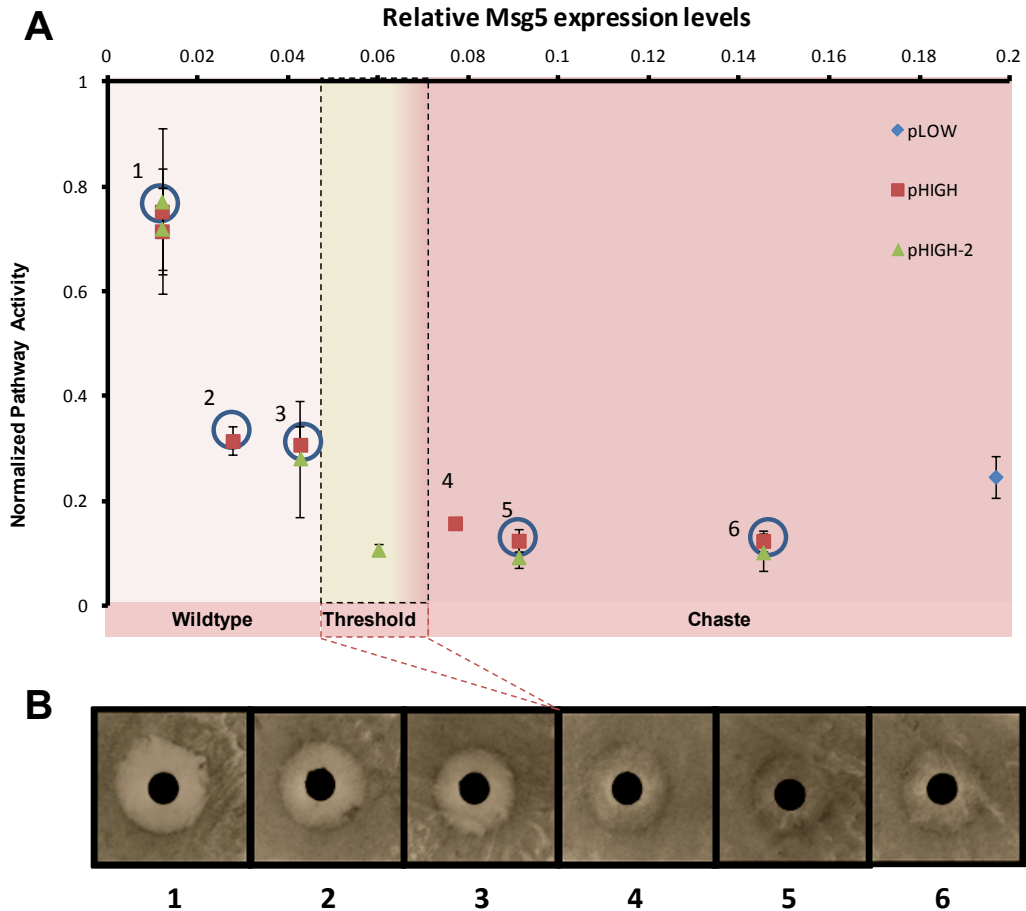
Supplementary Figure 2.7. Constitutive expression of Msg5 routes cells to for entire range of promoter strengths. Within the range of promoter strengths, Msg5 expression is above the threshold required for routing to the chaste fate.



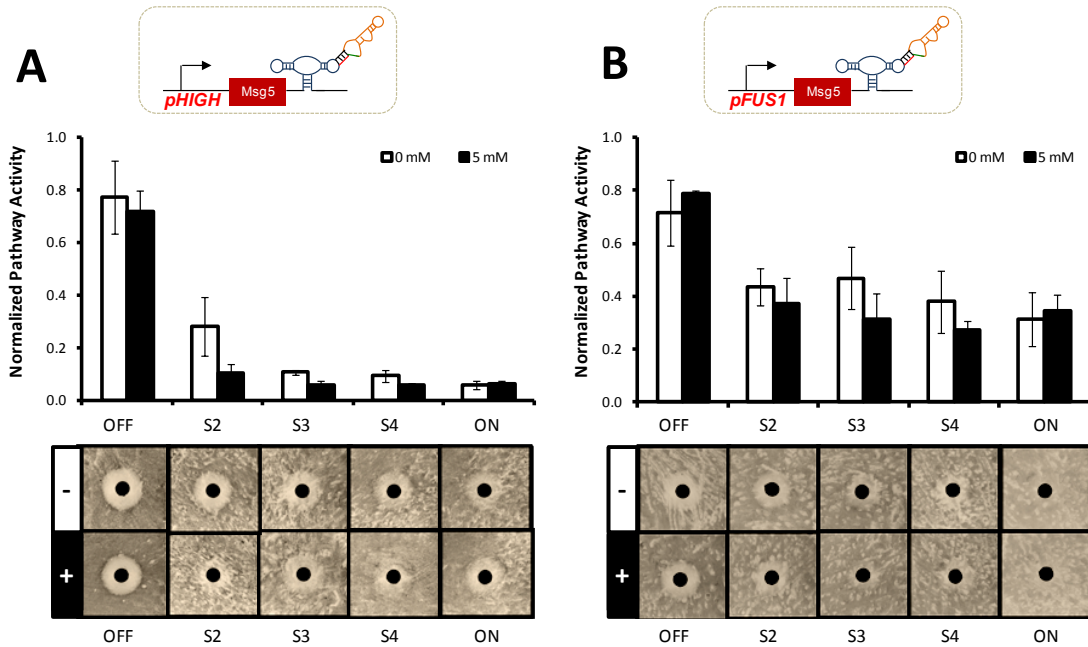
Supplementary Figure 2.8. Histograms show population distribution differences for constitutive and feedback network diverters. A. Histogram for pHIGH Msg5 ON results in a significant increase in the low pFUS1-GFP population relative to OFF. **B.** A low pFUS1-GFP population is minimal in both ON and OFF controls for pFUS1-Msg5. **C.** Histograms evaluating only the high pFUS1-GFP population for pHIGH-Msg5 ON and OFF has populations that mirror pFUS1-Msg5 ON and OFF, respectively, in **D.**



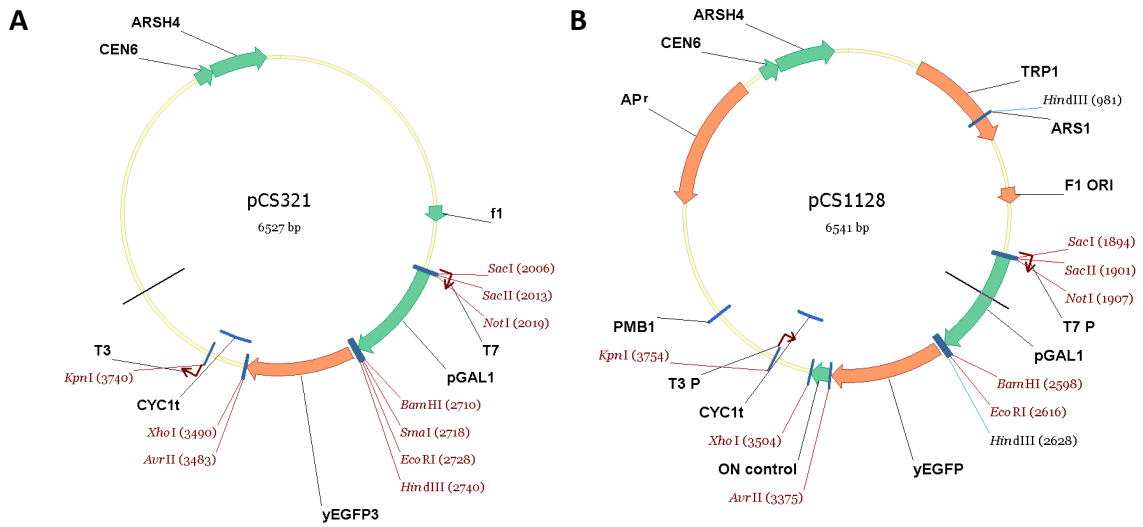
Supplementary Figure 2.9. Neglecting the low pFUS1-GFP population, both feedback architectures show similar mean levels of pathway activity are required for diverting pathway response to the chaste phenotype. Mean values were calculated excluding the low pFUS1-GFP population.



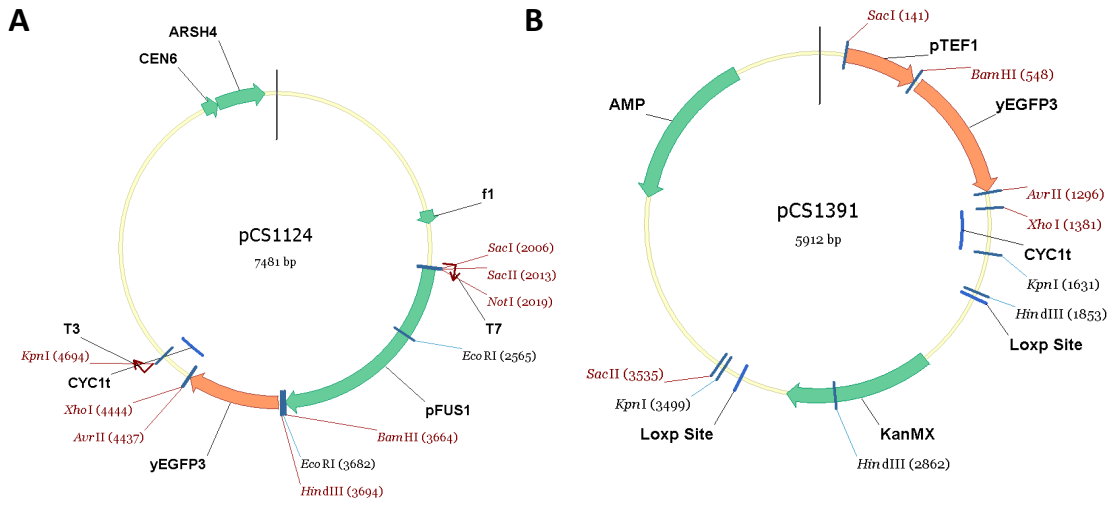
Supplementary Figure 2.10. Tracing the pathway response curve to constitutive Msg5 expression including the low GFP population shows similar transitory range for fate divergence. A. Pathway activity significantly decreases from 1% to 10%. B. Above 8% expression cells adopt the chaste fate. Plate data correspond to points with numbered circles in A selected from the pHIGH-SX data set (Figure 8A). Mean values of pathway activity were calculated including the low pFUS1-GFP population. Relative Msg5 expression was calculated from the relative promoter strengths (Supplementary figure 1) paired with the various switches (Supplementary Figure 2) relative to the pHIGH promoter paired with the ON switch control.



Supplementary Figure 2.10. Theophylline-inducible negative network diverters of different architectures conditionally route cells to the chaste phenotype.



Supplementary Figure 2.11. Original plasmids for construction of molecular network diverter and reporters. A. pCS321 B. pCS1128.



Supplementary Figure 2.12. A. pCS1124 B. pCS1391

Supplementary tables

Supplementary Table 2.1 GFP plasmids

pCS #	pKG#	Cassette	3'UTR	Marker
1128		pGAL1-YEGFP-CYC1t	sTRSV Ctrl	TRP
321		pGAL1-YEGFP-CYC1t	Empty	URA
1124		pFUS1 -YEGFP-CYC1t	Empty	URA
1585		pTEF1 -YEGFP-CYC1t	Empty	URA
	79	pTEF7 -YEGFP-CYC1t	Empty	URA
	80	pCYC1 -YEGFP-CYC1t	Empty	URA
	78	pADH1 -YEGFP-CYC1t	Empty	URA
	74	pSTL1-yEGFP-CYC1t	Empty	URA

Supplementary Table 2.2 Primer sequences

Insert or PCR Product	Primer Name	Sequence
pTEF7	pTEF7-FWD	5'- AA GAGCTC ATA GCT TCA AAA TGT CTC TAC TCC TTT TT
	pTEF7-REV	5'- AAA GGATCC AAC TTA GAT TAG ATT GCT ATGCTT TCT TTC C
pFUS1	pDS71.FUS1-FWD	5'-TTT GCGGCCGC CCA ATC TCA GAG GCT GAG TCT
	pDS71.pFUS1-REV	5'-TTT GGATCC TTT GAT TTT CAG AAA CTT GAT GGC
pADH1	pADH1-FWD	5'- AA GAGCTC AGC TCG ATA TCC TTT TGT TGT TTC C
	pADH1-REV	5'- AA GGATCC ATT GTA TGC TTG GTA TAG CTT GAA ATA TTG TG
pCYC1	pCYC1-FWD	5'- AA GAGCTC CTC GGT ACC CTA TGG CAT GCA TGT
	pCYC1-REV	5'- AAA GGATCCACGAA TTGATCCGGTAATTTAGTGTGTG
pSTL1	pSTL1-FWD	5'-AA GAGCTC GAT TCT GAA ATA CTC CTT TTA CAA CCT TTG C
	pSTL1-REV	5'-AAA GGATCC GGT CTA AAA CTT TCT ATG TTC TAT TTT TC
Ste4	Ste4.k2.FWD	5'- AAA GGATCC A AT TAA TA ATG GCA GCA CAT CAG ATG GAC
	Ste4.REV	5'-AAA CCTAGGCTATTGATAACCTGGAGACCATA
Ste50	Ste50. k2.FWD	5' - AAA GGATCC A AT TAA TA ATG GAG GAC GGT AAA CAG G
	Ste50.REV	5- AAA CCTAGG TTA GAG TCT TCC ACC GGG G
Ste11	Ste11.K2.FWD	5'-AAAAAA GGATCC ATTAATA ATG GAA CAG ACA CAA ACA GCA GAG
	Ste11.Stop.REV	5'- AAAA CCTAGG TCA AATTATGTGTGATCCAGCCATGGA
Ste7	Ste7.K2.FWD	5'-AAAAAA GGATCC ATTAATA ATG TTT CAA CGA AAG ACT TTA CAG AGA AGG
	Ste7.AvrII.REV	5'- AAAA CCTAGG TCA ATGGT TGA TCT TTC CGA T
Fus3	Fus3.K2.FWD	5'-AAAAAA GGATCC ATTAATA ATG CCA AAG AGA ATT GTA TAC AAT ATA TCC AG
	Fus3.A. STOP.REV	5'-AAAAAA CCTAGGCTA ACTA AAT ATT TCG TTC CAA ATG AGT TTC TTG AGG
Msg5	MSG5.K2.FWD	5'- AAA GGATCC A AT TAA TA GTGCACATGCAATTTAC
	Msg5.REV	5'-AAAA CCTAGG TTAAGGAAGAAACATCATCTG
Hog1	Hog1.FWD	5'-AAA GGATCC ATG ACC ACT AAC GAG GAA TTC ATT AGG A
	Hog1.k2.FWD	5'-AAA GGATCC A AT TAA TA ATG ACC ACT AAC GAG GAA TTC ATT AGG A
	Hog1.REV	5'-AAAA CCTAGG TTA CTG TTG GAA CT CATTAGCG
Pbs2	Pbs2. k2.FWD	5' - AAA GGATCC A AT TAA TA ATG GAA GAC AAG TTT GCT AAC CTC
	Pbs2.REV	5- AAA CCTAGGCTA TAA ACC ACC CAT ATG TAA TGC CG
Genomic Pbs2 PCR product	Pbs2. Chr.FWD	5' - GCAGATCGAGACGTTAATTTCTC
	Pbs2. Chr.REV	5- TCACGTGCCTGTTTGTCTTT
Ptc1	Ptc1.k2.FWD	5'- AAA GGATCC A AT TAA TA ATG AGT AAT CAT TCT GAA ATC TTA GAA AGG C
	Ptc1.REV	5- AAA CCTAGG TTA GAG GAA GAC AAC CAT GAC C
Genomic Ptc1 PCR product	Ptc1.Chr.FWD	5'- GGCAC TGCATTTA TCTTTTAAAAATC
	Ptc1. Chr.REV	5- TTGCGCGTTTATAACGGAT

Supplementary Table 2.3 Galactose-titration plasmids

pCS #	pKG#	Cassette	3'UTR	Marker
1625		pGAL1-Ste4-CYC1t	sTRSV Ctrl	TRP
1483		pGAL1-Ste11-CYC1t	sTRSV Ctrl	TRP
1484		pGAL1-Ste7-CYC1t	sTRSV Ctrl	TRP
1485		pGAL1-Fus3-CYC1t	sTRSV Ctrl	TRP
1486		pGAL1-Msg5-CYC1t	sTRSV Ctrl	TRP
	76	pGAL1-Ste50-CYC1t	sTRSV Ctrl	TRP
	77	pGAL1-Pbs2-CYC1t	sTRSV Ctrl	TRP
	158	pGAL1-Pbs2-CYC1t	sTRSV Ctrl	URA
	157	pGAL1-Hog1-CYC1t	sTRSV Ctrl	TRP
		pGAL1-Ptc1-CYC1t	sTRSV Ctrl	TRP

Supplementary Table 2.4 Primers for mutagenesis

Primer Name	Sequence	Purpose
Ste4. XhoImut.FWD	GTCACTGGTGTGCGATCGAGTCCAGATGG	Remove XhoI in Ste4
Ste4. XhoImut.REV	CCATCTGGACTCGATCGCACACCAATGAC	
Fus3-XHO.FWD	GGAGAAGATGTTCCCTAGAGTCAACCCGAAAGG	Remove XhoI in Fus3
Fus3-XHO.REV	CCTTTCGGGTTGACTCTAGGGAACATCTTCTCC	
Ste7-AvrII.FWD	GTAAC TGGAGAGTTTCCA CTAGGTGGGCATAACGA	Remove AvrII in Ste7
Ste7-AvrII.REV	TCGTTATGCCCACTAGTGGAAACTCTCCAGTTAC	
pCS1441.XhoImut.FWD	ATGCTGGCGCCCGCATCGAGAGATCTAAG	Remove XhoI from disintegrators
pCS1441.XhoImut.REV	CTTAGATCTCTCGATGCGGCCCGCCAGCAT	

Supplementary Table 2.5 Switch sequence information

Switches	Alias	Sequence	Basal Expression (0 mM)	Standard Induced Expression (5 mM or 1 mM)
ON	STRSV Ctrl	AAACAAACAAAAGCTGTCACCGGATGTGCTTTCCGGTAC GTGAGTCCGTGAGGACAGAAACAGCAAAAAGAAAAAT AAAAACTCGAG	100.0%	100.0%
OFF	sTRSV	AAACAAACAAAAGCTGTCACCGGATGTGCTTTCCGGTCTG ATGAGTCCGTGAGGACAGAAACAGCAAAAAGAAAAATA AAAAACTCGAG	1.2%	1.2%
S1	L2b8-a1 (aka LIN7-1)	AAACAAACAAAAGCTGTCACCGGAATCAAGGTCCGGTCT GATGAGTCCGTGTCCATACCAAGCATCGTCTTGATGCCCT TGGCAGGGACGGGACGGAGGACGAAACAGCAAAAAGAA AAAAATAAAAACCTCGAG	3.0%	8.0%
S2	L2b8-a1-t41 (aka LIN7-41)	AAACAAACAAAAGCTGTCACCGGAATCAAGGTCCGGTCT GATGAGTCCGTGTCCATACCAAGCATCGTCTTGATGCCCT TGGCAGACGGTAGACGGAGGACGAAACAGCAAAAAGAA AAAAATAAAAACCTCGAG	3.6%	12.7%
S3	L2b8-ta47 (aka S47)	AAACAAACAAAAGCTGTCACCGGATGTGCTTTCCGGTCTG ATGAGTCCGTGAGTATACCAAGCATCGTCTTGATGCCCT TGGCAGACTGTATACGGAGGACGAAACAGCAAAAAGAA AAAAATAAAAA	6.1%	33.6%
S4	L2b8 (aka L2b12)	AAACAAACAAAAGCTGTCACCGGATGTGCTTTCCGGTCTG ATGAGTCCGTGTCCATACCAAGCATCGTCTTGATGCCCT GGCAGGGACGGGACGGAGGACGAAACAGCAAAAAGAA AAAAATAAAAACCTCGAG	9.1%	36.7%
S5	L2b1	AAACAAACAAAAGCTGTCACCGGATGTGCTTTCCGGTCTG ATGAGTCCGTGTCCATACCAAGCATCGTCTTGATGCCCTG GACGGGACGGGACGAGGACGAAACAGCAAAAAGAAAA ATAAAAA	39.8%	75.3%
S1tc	L2b12tc-11	AAACAAACAAAAGCTGTCACCGGATGTGCTTTCCGGTCTG ATGAGTCCGTGTGTTGAAAAATACCAAGATTTTCGATCTGG AGAGGTGAAGAAATTCGACCACTCAATTCACCGGAGGA CGAAACAGCAAAAAGAAAAATAAAAACCTCGAG	3.7%	4.8%
S2tc	L2b8tc-a1 (aka L2b12tc-1)	AAACAAACAAAAGCTGTCACCGGAATCAAGGTCCGGTCT GATGAGTCCGTGTCCAAAAATACCAAGATTTTCGATCTG GAGAGGTGAAGAAATTCGACCACTGGACGGGACGGAGG ACGAAACAGCAAAAAGAAAAATAAAAACCTCGAGCC	3.0%	10.8%
S4tc	L2b8tc (aka L2b12tc)	AAACAAACAAAAGCTGTCACCGGATGTGCTTTCCGGTCTG ATGAGTCCGTGTCCAAAAATACCAAGATTTTCGATCTGG AGAGGTGAAGAAATTCGACCACTGGACGGGACGGAGGA CGAAACAGCAAAAAGAAAAATAAAAACCTCGAG	8.4%	43.9%
S3tc	L2b12tc-NheI- L2bOFF1 (aka Stc-OFF1)	AAACAAACAAAAGCTGTCACCGGATGTGCTTTCCGGTCTG ATGAGTCCGTGTCCAAAAATACCAAGATTTTCGATCTGG AGAGGTGAAGAAATTCGACCACTGGACGGGACGGAGGA CGAAACAGCAAAAAGAAAAATAAAAAGCTAGGAAAC AAACAAAAGCTGTCACCGGATGTGCTTTCCGGTCTGATGA GTCCGTGTGCTGATACCAAGCATCGTCTTGATGCCCTGG CAGCAGTGGACGAGGACGAAACAGCAAAAAGAAAAAT AAAAA	4.2%	21.2%

Supplementary Table 2.6 Msg5 plasmids

pX-Msg5-CYC1t			
pCS #	pKG#	Promoter	3'UTR
	88	pADH1	Empty
	145	pCYC1	Empty
	89	pTEF7	Empty
1487		pFUS1	Empty
	200	pADH1	ON
	154	pCYC1	ON
	123	pTEF7	ON
	121	pFUS1	ON
	199	pTEF1	ON
pFUS1-Msg5-CYC1t			
pCS #	pKG#	Parent	3'UTR
	121	pCS1487	ON
	45	pCS1487	S5
	48	pCS1487	S4
	286	pCS1487	S3
	220	pCS1487	S2
	168	pCS1487	S1
	137	pCS1487	OFF
pTEF7-Msg5-CYC1t			
pCS #	pKG#	Parent	3'UTR
	123	pKG89	ON
	112	pKG89	S5
	122	pKG89	S4
	293	pKG89	S3
	219	pKG89	S2
	169	pKG89	S1
	136	pKG89	OFF

Supplementary Table 2.7 Ste4 plasmids

pX-Ste4-CYC1t		
pKG#	Promoter	3'UTR
90	pADH1	Empty
87	pTEF7	Empty
84	pFUS1	Empty
159	pADH1	ON
203	pCYC1	ON
144	pTEF7	ON
173	pFUS1	ON
201	pTEF1	ON
pFUS1-Ste4-CYC1t		
pKG#	Parent	3'UTR
228	pKG227	ON
234	pKG227	S4tc
298	pKG227	S3tc
227	pCS2094	S2tc
274	pKG227	S1tc
233	pKG227	OFF
pFUS1-Ste4-CYC1t		
pKG#	Parent	3'UTR
173	pKG84	ON
215	pKG84	S5
64	pKG84	S4
161	pKG84	S2
176	pKG84	S1
124	pKG84	OFF
95	pKG84	S5tc
189	pKG84	S4tc
179	pKG84	S2tc
180	pKG84	S1tc
pTEF7-Ste4-CYC1t		
pKG#	Parent	3'UTR
144	pKG87	ON
272	pKG87	S4tc
296	pKG87	S3tc
177	pKG87	S2tc
178	pKG87	S1tc
152	pKG87	OFF
213	pKG87	S5tc
214	pKG87	S4tc
153	pKG87	S2tc
198	pKG87	S1tc
pADH1-Ste4-CYC1t		
pKG#	Parent	3'UTR
159	pKG90	ON
86	pKG90	S5
99	pKG90	S4
172	pKG90	S2
171	pKG90	S1
160	pKG90	OFF
pTEF7-Ste4-CYC1t		
pKG#	Parent	3'UTR
321	pCS1128	S4tc
295	pCS1128	S3tc
188	pCS1128	S2tc
182	pCS1128	S1tc
181	pCS1128	OFF

Supplementary Table 2.8 Plasmids for strain construction

pCS #	pKG#	Cassette	Integration Loci	Marker
1543		pCS1439 with XhoI removed; disintegrator [37]	FCY1	URA
	98	pCS1543 + pSTL1 -YEGFP-CYC1t	FCY1	URA
1391		LoxP Integrating plasmid [35]	Primer-specific	G418
	100	pCS1391+pFUS1-yEGFP-CYC1t	Primer-specific	G418

Supplementary Table 2.9 Yeast strains

CSY#	KG#	Description
364		EY1119 from [36]; W303a Δ sst1 Δ kss1::HIS3
408		CSY364 Δ gal2::KanR
532		CSY364 Δ gal2::pFUS1-GFP-CYC1t-loxP-KanR
840	144	CSY364 Δ trp1::pFUS1-yEGFP3-CYC1t-loxP-KanR
	145	CSY364 Δ gal21::pFUS1-yEGFP3-CYC1t-loxP-KanR
	139	CSY408 FCY1::pSTL1-GFP-CYC1t

Supplementary Table 2.10 Primers for integration

Loci	Sequence	Direction
GAL2	ATGCACCTTATTCAATTATCATCAAGAATAGTAATAGTTAAGTAAACACAAGATTAAACATAGATTGTACTGAGAGTGCAC	FWD
	ATGATAATTAAAATGAAGAAAAACGTCACTCATGAAAAATTAAAGAGAGATGATGGAGCGGACTCACTATAGGGAGACC	REV
TRP	GTATACGIGATTAAACACACAAAGGCAGCTTGGAGTATGTCTGTATTAATTTACAGGAAGATTGTACTGAGAGTGCAC	FWD
	TTGCTTTTCAAAGGCCTGCAGGCAAGTGCACAAACAATACTTAAATAAATACTACTCAGCGACTCACTATAGGGAGACC	REV